

The ELISA assay was carried out according as a previous report [7]. Bound chimeric antibodies were detected using a peroxidase-labeled anti-human IgG antibody (Cappel, USA). Antibody production was measured by specific quantitative ELISA using anti-human Igk chain antibody for capture and a peroxidase-labeled anti-human IgG (Fc) antibody (Zymed, USA) for detection. Purified human IgG₁ or IgG₄ (The Binding Site, UK) was used as a standard.

2.4. Western blotting

Standard procedures were used to analyze the size and IgG subclass of the chimeric antibodies. Supernatants containing 20 ng antibodies were subjected to SDS-PAGE under reducing or non-reducing conditions. Proteins were then transferred to an Immun-Blot™ PVDF membrane (BIO-RAD, USA) at 180 mA for 3 h. Blots were incubated for 1 h at room temperature with the various mAbs and were developed by ECL-plus (Amersham Pharmacia Biotech, Sweden). The following mAbs were used for the first reaction; anti-human Igγ chain antibody (Sigma, USA), anti-human Igκ chain antibody (Sigma, USA), anti-human IgG₁ antibody (BD Biosciences, USA), anti-human IgG₄ antibody (BD Biosciences, USA), a peroxidase-labeled donkey anti-chicken IgG antibody (Chemicon International, USA), and a peroxidase-labeled goat anti-human IgG antibody (Cappel, USA). A peroxidase-labeled rabbit anti-goat IgG antibody and a goat anti-mouse IgG antibody (Southern Biotech, USA) were used for the second reaction.

2.5. Determination of antigen binding affinities

The antigen binding affinities of the chimeric antibody (C/H1-Hu9) and the parental chicken antibody (HUNN1) was estimated using Biacore 2000 (Biacore AB, Sweden). A research-grade sensor chip CM5 and the Amine coupling kit containing *N*-hydroxysuccinimide, *N*-ethyl-*N'*-(3-dimethylaminopropyl) carbodiimide hydrochloride and ethanolamine hydrochloride were obtained from Biacore AB. Affinity purified goat anti-chicken IgG (Fc) antibody (Bethyl, USA) or affinity purified rabbit anti-human IgG (Fc) antibody (Rockland, USA) was immobilized onto the sensor chip with the use of the coupling kit according to the manufacturer's protocol. Binding assays were performed by the injection of 20 μl of the chicken antibody (10 μg/ml) or the chimeric antibody (10 μg/ml) at a flow rate of 10 μl/min, followed by 50 μl of varying concentration (12.5, 25, 50, 100 nM) of recombinant mouse PrP (Prionics, Switzerland) at a flow rate of 50 μl/min. Each data set was double-referenced and fit globally to a 1:1 interaction model using BIA evaluation software ver. 3.0 (Biacore AB).

3. Results and discussion

The expression vectors constructed in this study were designed for cloning all chicken antibody genes generated from hybridoma or phage display libraries. Therefore, we selected cloning sites that exhibited low cutting frequencies. We examined the restriction sites in the 80 heavy chain V region genes and the 167 light chain V region genes found in the GenBank and those generated in our laboratory [7]. *HindIII*, *AscI* and *BamHI* were then selected for cloning the V regions because no restriction sites for these enzymes were identified in the chicken antibodies.

Mammalian expression vectors were constructed; pcSLCγ1 and pcSLCγ4 for Ig heavy chain expression, and pcSLCκ for Ig light chain expression (Fig. 1). The pcSLCγ1 and pcSLCγ4 vectors are about 7.1 kb and contain the human Cγ1 and Cγ4 genes, respectively, as well as the Zeocin resistance gene as a selection maker. The pcSLCκ vector is about 6.3 kb and contains the human Cκ gene as well as the neomycin resistance gene as a selection marker. All vectors have a strong cytomegalovirus promoter, modified chicken secretory leader with Kozak sequence, bovine growth hormone polyadenylation site, ampicillin resistance gene, and an origin of replication. The myc epitope and polyhistidine tag are not translated as they are positioned downstream of the stop codon.

In order to involve or avoid effector functions, it is important to carefully select Ig isotypes. The IgG₁ and IgG₃ subclasses are known to exhibit potent effector function, complement activation, and promote antibody-dependent cell-mediated cytotoxicity through interaction with specific Fc receptors [17]. On the other hand, the IgG₄ subclass is deficient in complement activation and has little or no affinity for Fc receptors.

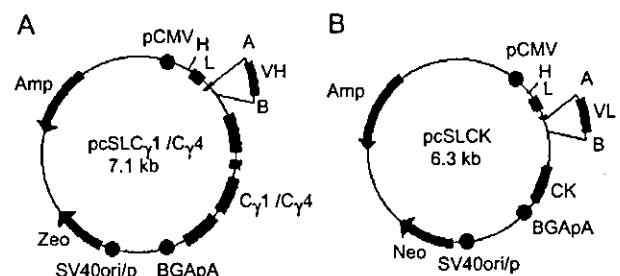


Fig. 1. Structure of chicken–human chimeric antibody expression vectors. (A) Heavy chain expression vectors, pcSLCγ1 and pcSLCγ4. (B) Light chain expression vector, pcSLCκ. Codes: L = leader, VH = heavy chain variable gene, VL = light chain variable gene, Amp = gene for ampicillin resistance, Zeo = gene for zeocin resistance, Neo = gene for neomycin resistance, BGH = bovine growth hormone, pA = polyadenylation site, pCMV = cytomegalovirus promoter, SV40ori/p = SV40 origin and promoter, A = *AscI*, B = *BamHI*, E = *EcoRI*, K = *KpnI*, N = *NorI*, X = *XhoI*.

Therefore, we constructed both the pcSLC γ 1 and pcSLC γ 4 vectors.

Human constant region genes were cloned from the genomic DNA of a healthy donor. Genomic constructs were used for the constant (C) regions rather than cDNA because genomic DNA includes cloning sites located within the introns and results in increased expression levels [18–20]. Our vectors contain part (more than 150 bp) of the human J–C introns, which include a splice acceptor site and branch point lariat signal. The deduced amino acid sequences of cloned C γ 1 and C κ were identical to those previously reported (GenBank accession number: C γ 1 Z17370, C κ NG_000834), while that of C γ 4 had one amino acid substitution (L325P) when compared with a previous report (C γ 4 AF237586), but this was a known polymorphism (either L or P).

Both heavy and light chain expression vectors have two sets of cloning sites; one (*Hind*III/*Bam*HI) for V regions derived from hybridomas, and the other (*Asc*I/*Bam*HI) for V regions selected from the phage display library. The 5'-cloning *Hind*III site is located upstream of the leader sequence, while the *Asc*I site is introduced by site-directed mutagenesis in the second exon of it. The deduced amino acid sequence of the leader sequence was thus slightly altered, but no effect on secretion was observed (data not shown). The 3'-cloning *Bam*HI site is located in the 5'-intron of the C region. Therefore, any chicken V region can be introduced into the expression vectors without amino acid substitution.

Expression levels of these vectors were tested under both transient and stable transfection conditions. As the source of the V regions, two different antibodies were used; HUNN1, which was derived from a hybridoma, and phAb3-15, which was an scFv selected from a phage display library [7]. For transient transfection, heavy chain expression vectors (pcSLC γ 1 or pcSLC γ 4) and light chain expression vector (pcSLC κ) were co-transfected into COS-7 cells, and antibody production was detected by specific quantitative ELISA. Complete antibodies were secreted into the culture medium and expression levels ranged from 1.5 to 2.5 μ g/ml after three days of culture (data not shown). For stable transfection, expression vectors were co-transfected into CHO-K1 cells. Stable transfectants were selected by culturing cells in the presence of Zeocin and Geneticin. Among antibody producing cells, several clones that had high levels of production were selected and their production levels were estimated by specific quantitative ELISA. Production levels ranged from 3.5 to 16.4 μ g/10⁶ cells/day (Fig. 2). Expression levels of COS-7 cells in previous reports typically ranged from 0.1 to 4.0 μ g/ml after two or three days of culture [19,21–23]. On the other hand, expression levels in stable CHO-K1 transfectants range from 0.3 to 5 μ g/10⁶ cells/day without gene amplification [19,23–26]. Therefore, our expression

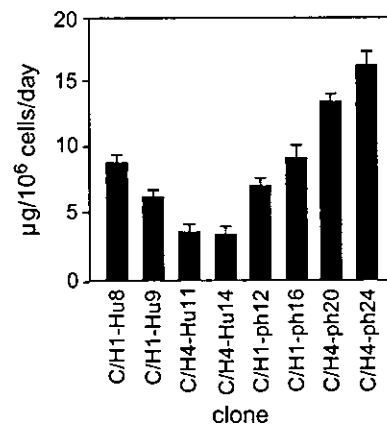


Fig. 2. Chimeric antibody production of transfected CHO cells. Supernatants were harvested from 10⁶ cells cultured for 24 h, and assayed for production levels by specific quantitative ELISA (see Section 2). Purified human IgG₁ or IgG₄ (The Binding Site, UK) were used as standards. HU clones possess the chicken V regions from HUNN1 hybridoma with human C κ and C γ 1 (C/H1-HU8 and C/H1-HU9) or human C κ and C γ 4 (C/H4-HU11 and C/H4-HU14). Ph clones possess the chicken V regions from phAb3-15 with human C κ and C γ 1 (C/H1-ph12 and C/H1-ph16) or human C κ and C γ 4 (C/H4-ph20 and C/H4-ph24).

vectors achieved good expression levels with both transient and stable transfection.

The structure and specificity of the chimeric antibodies in culture supernatants were determined by Western blot analysis (Figs. 3 and 4). Clone C/H1-ph16 possessed the chicken V regions derived from phAb3-15 and human C κ and C γ 1 as constant regions. Clone C/H4-ph24 was the same as C/H1-ph16, except for possessing C γ 4 instead of C γ 1. Under non-reducing conditions, the size of the completely assembled



Fig. 3. Western blot analysis for structure and size of chimeric antibodies. Culture supernatants containing 20 ng of antibodies were run on 10% SDS-PAGE gels under non-reducing conditions (A) and on 12.5% SDS-PAGE gels under reducing conditions (B). Proteins were transferred to nitrocellulose membranes and reacted with specific antibodies as follows. (A) A peroxidase-labeled anti-human IgG antibody. (B) Lanes 1 and 2, anti-human Igy antibody; lane 3 and 4, anti-human Igk antibody. Lanes A-1, B-1 and B-3, culture supernatants from C/H1-ph16 cell line; lanes A-2, B-2 and B-4, culture supernatants from C/H4-ph24 cell line.

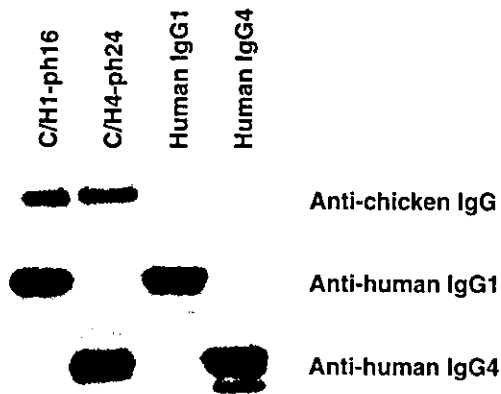


Fig. 4. Western blot analysis for specificity of chimeric antibodies. Culture supernatants containing 20 ng of antibodies were run under non-reducing conditions, and were transferred and probed. Regions of membranes containing chimeric antibodies are shown. Upper, reacted with anti-chicken IgG antibody; middle, anti-human IgG₁ antibody; lower, anti-human IgG₄ antibody.

antibodies was detected (Fig. 3 A). Supernatants from C/H4-ph24 also contained incompletely assembled antibodies, which were half the weight of the completely assembled antibodies (Fig. 3A, lane 2). This appears to be a general property of human IgG₄ molecules [27,28]. Under reducing conditions, the H and L chains were shown to have weights of approximately 50 and 25 kDa, respectively (Fig. 3 B). As shown in Fig. 4, supernatants from C/H1-ph16 reacted with anti-chicken IgG and anti-human IgG₁ antibody, but not with anti-human IgG₄ antibody. On the other hand, supernatants from C/H4-ph24 reacted with anti-chicken IgG and anti-human IgG₄ antibody but not with anti-human IgG₁ antibody. These results confirm that the produced antibodies are of the predicted size, structure and specificity.

To determine the chimeric antibody retain the binding activity to the antigen, the affinity of the chimeric antibody (C/H1-Hu9) and the parental chicken antibody (HUNN1) were measured by BIAcore 2000. The calculated K_D for the chimeric antibody was 3.3 nM whereas that for the parental chicken antibody was 2.7 nM. These results demonstrate that chimeric antibody retain the same binding affinity as the parental chicken antibody.

4. Conclusion

We described the construction of the novel expression vectors pcSLC γ 1, pcSLC γ 4 and pcSLC κ . Using these expression vectors, any chicken–human chimeric antibody can easily be constructed by simply replacing the V regions. The characteristics of our vectors are summarized as follows; (1) any chicken V regions that are prepared from hybridomas or a phage display library

can be easily introduced; (2) the V regions can be kept intact and can be expressed in different Ig isotypes; (3) these vectors can express under both transient and stable transfection conditions. Thus, the chicken–human chimeric antibody expression system presented here opens the door for clinical application of chicken mAbs.

Acknowledgment

This work was supported by a Grant-in-Aid from the Bio-oriented Technology Research Advancement Institution [BRAIN].

References

- Kohler G, Miltein C. Continuous culture of fused cells secreting antibody of predefined specificity. *Nature* 1975;256:495–7.
- Song CS, Yu JH, Bai DH, Hester PY, Kim KH. Antibodies to the alpha-subunit of insulin receptor from the eggs of immunized hens. *J Immunol* 1985;135:3354–9.
- Goueli SA, Hanten J, Davis A, Ahmed K. Polyclonal antibodies against rat liver cytosolic casein kinase II (CK-2) cross-react with CD-2 from other tissues and nuclear for (PK-N2) of the enzyme. *Biochem Int* 1990;21:685–94.
- Asaoka H, Nishinaka S, Wakamiya N, Matsuda H, Murata M. Two chicken monoclonal antibodies specific for heterophil Hanganutziu-Deicher antigen. *Immunol Lett* 1992;32:91–6.
- Matsushita K, Horiuchi H, Furusawa S, Horiuchi M, Shinagawa M, Matsuda H. Chicken monoclonal antibodies against synthetic bovine prion protein peptide. *J Vet Med Sci* 1998;60:777–9.
- Matsuda H, Mitsuda H, Nakamura N, Furusawa S, Mohri S, Kitamoto T. A chicken monoclonal antibody with specificity for the N-terminal of human prion protein. *FEMS Immunol Med Microbiol* 1999;23:189–94.
- Nakamura N, Shuyama A, Hojyo S, Shimokawa M, Miyamoto K, Kawashima T, Aosasa M, Horiuchi H, Furusawa S, Matsuda H. Establishment of chicken monoclonal antibody panel against prion protein. *J Vet Med Sci* 2004;66:807–14.
- McCormack WT, Tjoelker LW, Thompson CB. Immunoglobulin gene diversification by gene conversion. *Prog Nucleic Acid Res Mol Biol* 1993;45:27–45.
- Boulianne GL, Hozumi N, Shulman MJ. Production of functional chimaeric mouse/human antibody. *Nature* 1984;312:643–6.
- Morrison S, Johnson MJ, Herzenberg LA, Oi VT. Chimeric human antibody molecules: Mouse antigen-binding domains with human constant region domains. *Proc Natl Acad Sci USA* 1984; 81:6851–5.
- Sahagan BG, Dorai H, Saltzger-Muller J, Toneguzzo F, Guindon CA, Lilly SP, McDonald KW, Morrissey DV, Stone BA, Davis GL, McIntosh PK, Moore. A genetically engineered murine/human chimeric antibody retains specificity for human tumor-associated antigen. *J Immunol* 1986;137: 1066–74.
- Liu AY, Robinson RR, Hellström KE, Murray Jr ED, Chang CP, Hellström I. Chimeric mouse-human IgG1 antibody that can mediated lysis of cancer cells. *Proc Natl Acad Sci USA* 1987;84: 3439–43.
- Sun LK, Curtis P, Rakowicz-Szulczynska E, Ghrayed J, Chang N, Morrison SL, Koprowski H. Chimeric antibody with human constant regions and mouse variable regions directed against

- carcinoma-associated antigen 17-1A. *Proc Natl Acad Sci USA* 1987;84:214–8.
14. Orlandi R, Gussow DH, Jones PT, Winter G. Cloning of immunoglobulin variable domains for expression by the polymerase chain reaction. *Proc Natl Acad Sci* 1989;86:3833–7.
 15. LoBuglio AF, Wheeler RH, Trang J, Haynes A, Rogers K, Harvey EB, Sun L, Ghayeb J, Khazaeli MB. Mouse/human chimeric monoclonal antibody in man: Kinetics and immune response. *Proc Natl Acad Sci USA* 1989;86:4220–4.
 16. Glennie MJ, Johnson PWM. Clinical trials of antibody therapy. *Immunol Today* 2000;21:403–10.
 17. Burton DR, Woof JM. Human antibody effector function. *Adv Immunol* 1992;51:1–84.
 18. Chapman BS, Thayer RM, Vincent KA, Haigwood NL. Effect of intron A from human cytomegalovirus (Towne) immediate-early gene on heterologous expression in mammalian cells. *Nuc Acid Res* 2001;19:3979–86.
 19. Fouser LA, Swanberg SL, Lin B-Y, Benedict M, Kelleher K, Cumming DA, Riedel GE. High level expression on a chimeric anti-ganglioside GD2 antibody: genomic kappa sequences improve expression in COS and CHO cells. *Biotechnology (NY)* 1992;10:1121–7.
 20. Chan K-T, Cheng SC-S, Xie H, Xie Y. A humanized monoclonal antibody constructed from intronless expression vectors targets human hepatocellular carcinoma cells. *Biochem Biophys Res Commun* 2001;284:157–67.
 21. Ames RS, Tornetta MA, Deen K, Jone CS, Swift AM, Ganguly S. Conversion of murine Fabs isolated from a combinatorial phage display library to full length immunoglobulins. *J Immunol Methods* 1995;184:177–86.
 22. Norderhang L, Olafsen T, Michaelsen TE, Sandlie I. Versatile vectors for transient and stable expression of recombinant antibody molecules in mammalian cells. *J Immunol Methods* 1997;204:77–87.
 23. Persic L, Roberts A, Wilton J, Cattaneo A, Bradbury A, Hoogenboom HR. An integrated vector system for the eukaryotic expression of antibodies or their fragments after selection from phage display libraries. *Gene* 1997;187:9–18.
 24. Reff ME, Carner K, Chamber KS, Chinn PC, Leonard JE, Raab R, Newman RA, Hanna N, Anderson DR. Depletion of B cells in vivo by a chimeric mouse human monoclonal antibody to CD20. *Blood* 1994;83:435–45.
 25. Bianchi AA, McGrew JT. High-level expression of full-length antibodies using trans-complementing expression vectors. *Biotechnol Bioeng* 2003;84:439–44.
 26. Chin J, Sohn Y, Lee SH, Park YI, Choi MJ. Production of neutralizing human monoclonal antibody directed to tetanus toxin in CHO cell. *Biologicals* 2003;31:45–53.
 27. Bebbington CR, Renner G, Thomson S, King D, Abrams D, Yarranton GT. High-level expression of a recombinant antibody from myeloma cells using a glutamine synthetase gene as an amplifiable selectable marker. *Biotechnology (NY)* 1992;10:169–75.
 28. King DJ, Adair JR, Angal S, Low DC, Proudfoot KA, Lloyd JC, Bodmer MW, Yarranton GT. Expression, purification and characterization of a mouse-human chimeric antibody and chimeric Fab' fragment. *Biochem J* 1992;281:317–23.

Heidenhain Variant of Creutzfeldt-Jakob Disease: Diffusion-Weighted MRI and PET Characteristics

Yoshihisa Tsuji, MD
Hiroshi Kanamori, MD
Gaku Murakami, MD
Masayuki Yokode, MD
Takahiro Mezaki, MD
Katsumi Doh-ura, MD
Ken Taniguchi, MD
Kozo Matsubayashi, MD
Hidenao Fukuyama, MD
Toru Kita, MD
Makoto Tanaka, MD

ABSTRACT

Creutzfeldt-Jakob disease (CJD) is characterized by rapidly progressive dementia with a variety of neurological disorders and a fatal outcome. The authors present a case with visual disturbance as a leading symptom and rapid deterioration in global cognitive functions. The cerebrospinal fluid was positive for 14-3-3 protein, and diffusion-weighted magnetic resonance imaging (MRI) showed marked hyperintensity in the parieto-occipital cortices, where hypometabolism was clearly detected on positron emission tomography (PET). Pattern-reversal visual evoked potentials showed prolonged P100 latencies and increased N75/P100 amplitudes. All these findings supported a diagnosis of the Heidenhain variant of CJD, whereas a long clinical course, a lack of myoclonus, and an absence of periodic synchronous discharges on electroencephalography were atypical. Diffusion-weighted MRI and PET in combination with visual evoked potential recording and 14-3-3 protein detection may be useful for the early diagnosis of CJD.

Key words: Creutzfeldt-Jakob disease, visual disturbance, 14-3-3 protein, diffusion-weighted MRI, PET, visual evoked potentials.

Tsuji Y, Kanamori H, Murakami G, Yokode MD,
Mezaki T, Doh-ura K, Taniguchi K,
Matsubayashi K, Fukuyama H, Kita T, Makoto T.
Heidenhain variant of Creutzfeldt-Jakob disease:
diffusion-weighted MRI and PET characteristics.
J Neuroimaging 2004;14:63-66.
DOI: 10.1177/1051228403258147

Creutzfeldt-Jakob disease (CJD) is a rare spongiform encephalopathy occurring sporadically in most cases. The diagnosis of CJD is based on clinical symptoms, such as rapidly progressive dementia, myoclonus, visual or cerebellar signs, pyramidal or extrapyramidal signs, and akinetic mutism, although the definite diagnosis of CJD requires pathological findings of the

brain.¹ Periodic synchronous discharges (PSDs) on electroencephalography (EEG) and the detection of 14-3-3 protein in the cerebrospinal fluid (CSF) further support clinical suspicion of CJD.¹⁻⁴ Furthermore, magnetic resonance imaging (MRI), particularly diffusion-weighted imaging (DWI), has been shown to be useful in diagnosing the disease.⁵⁻¹² Herein, we report a probable case of CJD in which neuroimaging techniques proved useful in the early diagnosis of the disease. Progressive dementia, visual disturbance, 14-3-3 protein in the CSF, and neuroimaging findings supported a diagnosis of CJD, but other clinical manifestations were atypical, including a long clinical course, the absence of myoclonus, and no PSDs on EEG.

Case Presentation

A 54-year-old woman noticed blurred vision and visual metamorphosis in August 2001. Her visual disturbance worsened, and she gave up driving a car. At 2 months, her family noticed that she had memory impairment and disorientation for time and place. She often lost her way around her house. Her cognitive deterioration rapidly progressed, and she felt difficulties in

Received March 31, 2003, and in revised form May 6, 2003. Accepted for publication May 9, 2003.

From the Departments of Geriatric Medicine (YT, HK, GM, MT), Neurology (TM), Functional Brain Imaging, Human Brain Research Center (HF), and Cardiovascular Medicine (TK), Graduate School of Medicine, Kyoto University, Kyoto, Japan; the Translational Research Center, Faculty of Medicine, Kyoto University (MY); the Department of Neuropathology, Neurological Institute, Kyushu University, Kyushu, Japan (KD); the Department of Psychiatry, Shoraiso National Hospital (KT); and the Center for Southeast Asian Studies, Kyoto University (KM).

Address correspondence to Makoto Tanaka, MD, Department of Geriatric Medicine, Graduate School of Medicine, Kyoto University, 54 Shogoin-Kawahara-cho, Sakyo-ku, Kyoto 606-8507, Japan. E-mail: makoto@kuhp.kyoto-u.ac.jp.

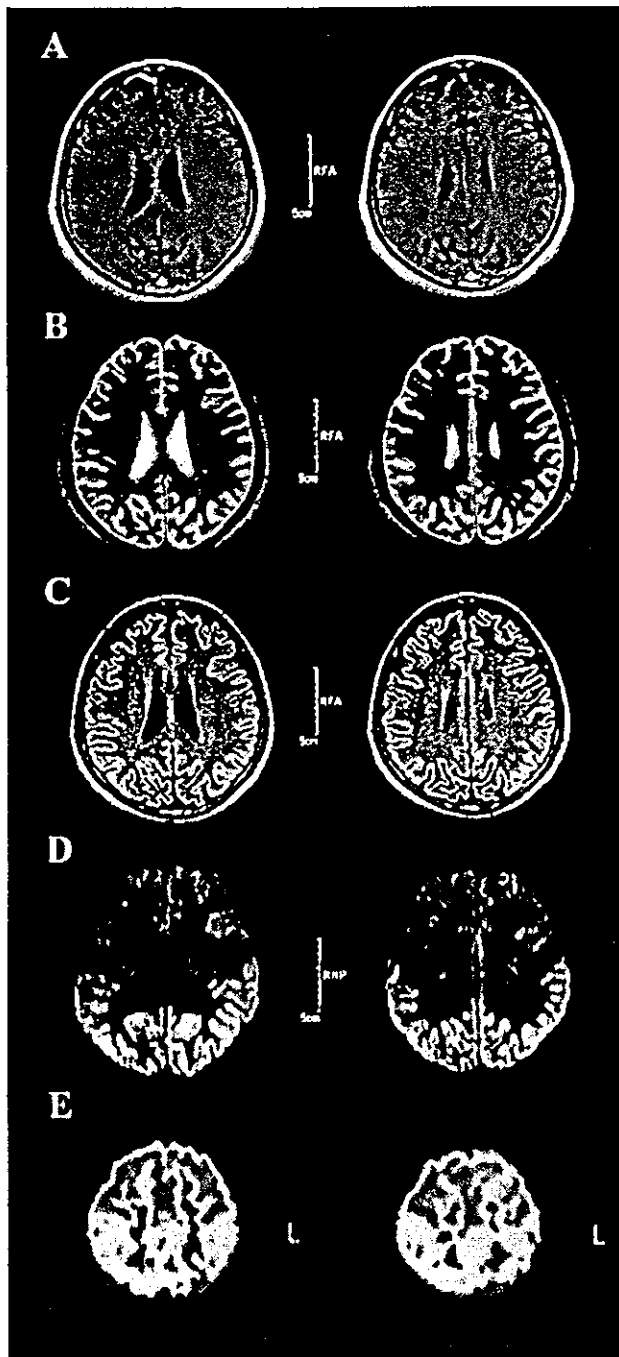
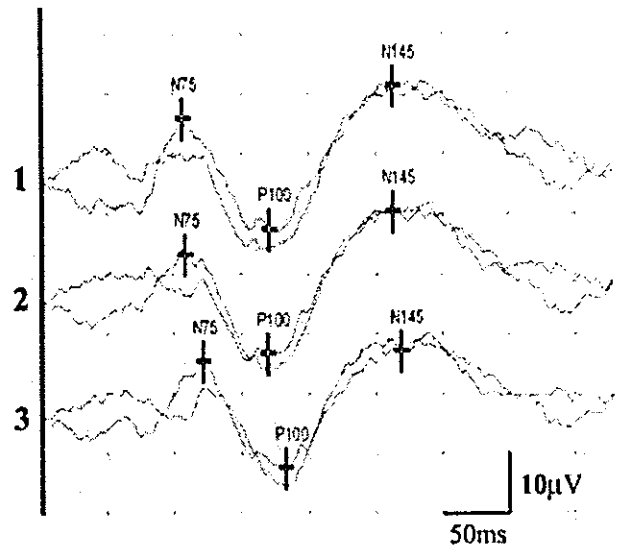


Fig 1. Magnetic resonance imaging (MRI) and positron emission tomography (PET) axial images. There was no atrophy, signs of cerebrovascular disease, or obvious signal abnormality on T1-weighted or T2-weighted MRI (A, B). High signal intensity in the parieto-occipital regions was detected on fluid-attenuated inversion recovery MRI (C), and the hyperintensity was most obvious on diffusion-weighted MRI (D). Low glucose metabolism was observed in the parieto-occipital regions as well as in the posterior cingulate cortex on PET (E). For the PET study, 5 mCi of [¹⁸F]-fluorodeoxyglucose were administered intravenously, and scanning was performed using GE Advance (GE Medical Systems, Milwaukee, WI). Semiquantitative measurements were used.

calculation, reading, writing, and cooking at the beginning of 2002. She was often unable to locate the bathroom in her house by March 2002.



	Latency (ms)	Latency (ms)	Latency (ms)		Amplitude (μV)	Amplitude (μV)
1	N75 106	P100 170	N145 262		N75P100 18.75	P100N145 24.11
2	N75 108	P100 169	N145 262		N75P100 17.03	P100N145 24.27
3	N75 121	P100 182	N145 268		N75P100 18.38	P100N145 20.16

Fig 2. Pattern-reversal visual evoked potentials (VEPs). Binocular full-field pattern-reversal VEPs revealed prolonged P100 latencies and increased N75/P100 amplitudes. The active electrodes were placed on the left (1), the median (2), and the right (3) occipital scalp.

When she was admitted to Kyoto University Hospital in April 2002, she complained only of visual disturbance. Her medical history included operations for appendicitis and uterocervical cancer. There was no family history of dementia or psychiatric disease. She was not taking any regular medications. A neurological examination disclosed memory impairment, disorientation, anomia, alexia, agraphia, acalculia, dressing apraxia, color agnosia, and visual metamorphosis. A cranial nerve examination was normal. There were no pyramidal, extrapyramidal, or cerebellar signs or involuntary movements, including myoclonus. Her score on the Mini-Mental State Examination was 12 of 30, and she obtained a total IQ score of 48 on the Wechsler Adult Intelligence Scale-Revised.

The results of a blood test and a CSF examination were unremarkable except for positive 14-3-3 protein in the CSF. Lactic or pyruvic acid was not elevated in the CSF, and paraneoplastic markers, including anti-Hu and anti-Yo, were not detectable either in serum or in the CSF. Notably, an MRI examination revealed symmetric, bilateral, cortical hyperintensity in the parieto-occipital regions (Figs 1C, 1D). DWI most strikingly showed abnormalities in these areas (Fig 1D). There was no mass effect, atrophy, or signs of cerebrovascular disease (Figs 1A-1D). Moreover, positron emission tomography (PET) demonstrated metabolic disturbance in the parietal, occipital, and posterior cingulate cortices (Fig 1E). EEG showed diffuse slowing without typical PSDs. Pattern-reversal visual evoked potentials (VEPs) showed prolonged P100 latencies and increased N75/P100 amplitudes (normal P100 latency < 132 milliseconds,

normal N75/P100 amplitude $< 10 \mu V^{13}$ (Fig 2). Genetic studies on the prion protein gene (PRNP) demonstrated no known mutations but disclosed homozygosity for methionine at the polymorphic codon 129. A brain biopsy could not be performed because we could not obtain permission from the patient's family.

At 16 months after the initial symptoms, limb and neck rigidity became apparent. At 20 months, she cannot recognize even her family members and has difficulty in oral communication because of the progression of agnosia and aphasia.

Discussion

Visual disturbance as a leading symptom, rapidly progressive dementia, and the detection of 14-3-3 protein in the CSF suggested a diagnosis of the Heidenhain variant of CJD.¹⁴ Methionine homozygosity at codon 129 of the PRNP gene was consistent with this subtype.¹⁵ However, this case did not fulfill the criteria for even possible CJD until the patient exhibited pronounced rigidity at 16 months after the initial symptoms.¹ This was due to the lack of some common clinical manifestations of CJD in this patient, including myoclonus, ataxia, and PSDs on EEG. This case not only suggests a heterogeneity of clinical presentation among patients with CJD but indicates difficulty in the early diagnosis of CJD without typical presentation. Currently used diagnostic criteria based on clinical symptoms and EEG findings may miss some CJD cases without typical sets of clinical manifestations, as in this case. Therefore, it is important to use neuroimaging and laboratory examinations for the early diagnosis of the disease.

Increased T2-weighted MRI signal has been described in the basal ganglia,^{5,8} and recently, cortical hyperintensity was shown on diffusion-weighted MRI in some CJD cases with typical clinical courses.^{6,7,10,11,16} Moreover, areas of signal abnormalities on diffusion-weighted MRI were well correlated with the neuropathologic findings of spongiform encephalopathy.¹⁰ In the present case, hyperintensity in the parieto-occipital lobes was clearly shown on diffusion-weighted MRI early in the clinical course, indicating that diffusion-weighted MRI is useful for the early diagnosis of CJD.

There has been a relatively limited number of reports describing PET studies of CJD.^{6,17,18} Henkel et al¹⁸ analyzed PET studies of 8 patients with CJD and found decreased glucose metabolism in the occipital lobe, cerebellum, or basal ganglia in addition to temporal or parietal cortical region. In the present case, metabolic disturbance was observed in the parietal, occipital, and posterior cingulate cortices. Although metabolic reductions in the parietal and posterior cingulate cortices are seen in other dementing diseases,^{19,20} the clear involvement of the occipital lobes differed from the typical pattern of disturbance detected in Alzheimer's disease,²⁰ which is the most frequent misdiagnosis of CJD.²¹ It may be more difficult to distinguish dementia with Lewy bodies (DLB) from CJD on PET, because significant metabolic reductions in the occipital cortex can be also seen in DLB.^{20,22} Diffusion-weighted MRI and 14-3-3 protein detection may be useful in the differential diagnosis of the 2 diseases.²³

VEPs may also provide a diagnostic aid for the early detection of CJD. According to previous reports, P100 latencies were increased or normal, but increased P100 amplitudes were the most frequent finding in CJD patients, particularly during the

early stages of the disease.^{13,24,25} Our case also showed increased P100 amplitudes at the early phase of the disease, thus indicating that VEP recording may be helpful, particularly in the early diagnosis of CJD without typical clinical presentation.

14-3-3 protein is expressed in all eukaryotic cells and participates in the regulation of diverse biological processes, including neuronal development, cell growth control, and cell cycling. There are 7 isoforms, 5 of which are present in neuronal cells and constitute nearly 1% of all soluble brain proteins.²⁶ The detection of 14-3-3 protein in the CSF probably reflects severe neuronal destruction.²³ 14-3-3 protein in the CSF has been shown to be a useful biochemical marker for CJD,^{2,4} and Zerr et al⁴ demonstrated that the specificity was even higher than that of PSDs on EEG. In the recent revised version of the French and European study criteria, positive 14-3-3 protein detection is considered as a criterion equivalent to a typical EEG.¹ According to the revised version, our patient was classified as probable CJD.

CJD may be a more heterogeneous group of disorders than has been recognized, and neuroimaging techniques, including diffusion-weighted MRI and PET, in combination with VEPs and 14-3-3 protein detection may be useful for the early diagnosis of CJD.

References

1. Brandel JP, Delasnerie-Lauprete N, Laplanche JL, Hauw JJ, Alperovitch A. Diagnosis of Creutzfeldt-Jakob disease: effect of clinical criteria on incidence estimates. *Neurology* 2000;54:1095-1099.
2. Hsich G, Kenney K, Gibbs CJ, Lee KH, Harrington MG. The 14-3-3 brain protein in cerebrospinal fluid as a marker for transmissible spongiform encephalopathies. *N Engl J Med* 1996;335:924-930.
3. Staffen W, Trinka E, Iglseder B, Pilz P, Homann N, Ladurner G. Clinical and diagnostic findings in a patient with Creutzfeldt-Jakob disease (type Heidenhain). *J Neuroimaging* 1997;7:50-54.
4. Zerr I, Pocchiari M, Collins S, et al. Analysis of EEG and CSF 14-3-3 proteins as aids to the diagnosis of Creutzfeldt-Jakob disease. *Neurology* 2000;55:811-815.
5. Finkenstaedt M, Szudra A, Zerr I, et al. MR imaging of Creutzfeldt-Jakob disease. *Radiology* 1996;199:793-798.
6. Na DL, Suh CK, Choi SH, et al. Diffusion-weighted magnetic resonance imaging in probable Creutzfeldt-Jakob disease: a clinical-anatomic correlation. *Arch Neurol* 1999;56:951-957.
7. Demaerel P, Heiner L, Robberecht W, Sciot R, Wilms G. Diffusion-weighted MRI in sporadic Creutzfeldt-Jakob disease. *Neurology* 1999;52:205-208.
8. Schroter A, Zerr I, Henkel K, Tschampa HJ, Finkenstaedt M, Poser S. Magnetic resonance imaging in the clinical diagnosis of Creutzfeldt-Jakob disease. *Arch Neurol* 2000;57:1751-1757.
9. Jacobs DA, Lesser RL, Mourelatos Z, Galetta SL, Balcer LJ. The Heidenhain variant of Creutzfeldt-Jakob disease: clinical, pathologic, and neuroimaging findings. *J Neuroophthalmol* 2001;21:99-102.
10. Mittal S, Farmer P, Kalina P, Kingsley PB, Halperin J. Correlation of diffusion-weighted magnetic resonance imaging with neuropathology in Creutzfeldt-Jakob disease. *Arch Neurol* 2002;59:128-134.

11. Rabinstein AA, Whiteman ML, Shebert RT. Abnormal diffusion-weighted magnetic resonance imaging in Creutzfeldt-Jakob disease following corneal transplantations. *Arch Neurol* 2002;59:637-639.
12. Eschweiler GW, Wormstall H, Widmann U, Naegele T, Bartels M. Correlation of diffusion-weighted magnetic resonance imaging with neurological deficits in sporadic Creutzfeldt-Jakob Disease. *Nervenarzt* 2002;73:883-886.
13. de Seze J, Hache JC, Vermersch P, et al. Creutzfeldt-Jakob disease: neurophysiologic visual impairments. *Neurology* 1998;51:962-967.
14. Kropp S, Schulz-Schaeffer WJ, Finkenstaedt M, et al. The Heidenhain variant of Creutzfeldt-Jakob disease. *Arch Neurol* 1999;56:55-61.
15. Parchi P, Giese A, Capellari S, et al. Classification of sporadic Creutzfeldt-Jakob disease based on molecular and phenotypic analysis of 300 subjects. *Ann Neurol* 1999;46:224-233.
16. Bahn MM, Parchi P. Abnormal diffusion-weighted magnetic resonance images in Creutzfeldt-Jakob disease. *Arch Neurol* 1999;56:577-583.
17. Grunwald F, Pohl C, Bender H, et al. 18F-fluorodeoxyglucose-PET and 99mTc-bicisate-SPECT in Creutzfeldt-Jakob disease. *Ann Nucl Med* 1996;10:131-134.
18. Henkel K, Zerr I, Hertel A, et al. Positron emission tomography with [(18)F]FDG in the diagnosis of Creutzfeldt-Jakob disease (CJD). *J Neurol* 2002;249:699-705.
19. Minoshima S, Giordani B, Berent S, Frey KA, Foster NL, Kuhl DE. Metabolic reduction in the posterior cingulate cortex in very early Alzheimer's disease. *Ann Neurol* 1997;42:85-94.
20. Minoshima S, Foster NL, Sima AA, Frey KA, Albin RL, Kuhl DE. Alzheimer's disease versus dementia with Lewy bodies: cerebral metabolic distinction with autopsy confirmation. *Ann Neurol* 2001;50:358-365.
21. Poser S, Mollenhauer B, Kraubeta A, et al. How to improve the clinical diagnosis of Creutzfeldt-Jakob disease. *Brain* 1999;122:2345-2351.
22. Lobotesis K, Fenwick JD, Phipps A, et al. Occipital hypoperfusion on SPECT in dementia with Lewy bodies but not AD. *Neurology* 2001;56:643-649.
23. Haik S, Brandel JP, Sazdovitch V, et al. Dementia with Lewy bodies in a neuropathologic series of suspected Creutzfeldt-Jakob disease. *Neurology* 2000;55:1401-1404.
24. Aguglia U, Farnarier G, Regis H, Oliveri RL, Quattrone A. Sensory evoked potentials in Creutzfeldt-Jakob disease. *Eur Neurol* 1990;30:157-161.
25. Finsterer J, Bancher C, Mamoli B. Giant visually-evoked potentials without myoclonus in the Heidenhain type of Creutzfeldt-Jakob disease. *J Neurol Sci* 1999;167:73-75.
26. Green AJ. Use of 14-3-3 in the diagnosis of Creutzfeldt-Jakob disease. *Biochem Soc Trans* 2002;30:382-386.

Clinical features of Creutzfeldt–Jakob disease with V180I mutation

K. Jin, MD; Y. Shiga, MD, PhD; S. Shibuya, MD, PhD; K. Chida, MD, PhD; Y. Sato, MD, PhD; H. Konno, MD, PhD; K. Doh-ura, MD, PhD; T. Kitamoto, MD, PhD; and Y. Itoyama, MD, PhD

Abstract—The authors describe the clinical features of Creutzfeldt–Jakob disease (CJD) with the causative point mutation at codon 180. The symptoms never started with visual or cerebellar involvement. The patients showed slower progression of the disease compared with sporadic CJD. They never showed periodic sharp and wave complexes in EEG. MRI demonstrated remarkable high-intensity areas with swelling in the cerebral cortex except for the medial occipital and cerebellar cortices. These characteristic MRI findings are an important clue for an accurate premortem diagnosis.

NEUROLOGY 2004;62:502–505

Approximately 10 to 15% of all Creutzfeldt–Jakob disease (CJD) cases are estimated to be familial.¹ Some of them are sporadic cases with no relevant family history because of incomplete genetic penetrance and the misdiagnosis of other affected family members. The clinical features depend on the genetic mutations. However, most patients demonstrate periodic sharp and wave complexes (PSWC) in EEG, an accepted diagnostic marker for CJD.

CJD with a causative point mutation of valine to isoleucine at codon 180 (V180I)^{2–5} is a type of familial CJD with no relevant family history. In case reports, the clinical features of CJD with V180I (CJD180) were different from those of sporadic CJD (sCJD). Therefore, the premortem clinical diagnosis was difficult, and the cases had been misdiagnosed as neurodegenerative disorders with dementia. We herein report the clinical features and characteristic MRI findings of five original cases of CJD180 together with a review of four reported cases.

Patients and methods. *Patients.* Nine patients including our five original patients and four other previously reported pathologically verified patients^{2–4} were studied retrospectively. The clinical features of these patients are shown in table 1. The previously reported case with a double mutation at codon 180 and codon 232 of the PRNP was excluded from this study because the codon 232 mutation might influence the clinical course.⁶ All nine had neither family history of dementia nor obvious iatrogenic exposure. Their PRNP analyses at codon 129 revealed that four had methionine homozygosity (MM129) and five had methionine/valine heterozygosity (MV129), in which the V180I mutation and valine at codon 129 were on different alleles.

The common histopathologic findings in the five pathologically verified patients were evident spongiform changes in all layers of the cerebral cortex with less prominent neuronal loss and gliosis without Kuru plaque. Immunohistochemical analysis showed

weak prion protein staining of the synaptic type in three of three patients examined.^{2,4,5}

Methods. We compared the clinical features, laboratory findings, and MRI findings of the 9 patients with those of 123 patients (25 were pathologically verified) with genetically verified sCJD, which were reported to the Japanese CJD Surveillance Committee.⁷ The PRNP analysis revealed that 116 of the 123 had MM129, 5 had MV129, and 2 had valine homozygosity at codon 129. We then compared the features between CJD180 and sCJD by dividing them into two groups: patients with MM129 and patients with MV129.

CSF was examined within 6 months from the onset for the differential diagnosis. The neuron-specific enolase (NSE) value in CSF was measured commercially using an ELISA method (SRL Laboratory, Tokyo, Japan), and a value of >35 ng/mL was considered positive.⁸ The 14-3-3 protein immunoassay was performed by western blot using polyclonal antibody SC-629 (Santa Cruz Biotechnology, Santa Cruz, CA). EEG using the International 10–20 method was examined repeatedly during the disease course.

In the MRI study, T1-weighted (T1), T2-weighted (T2), fluid-attenuated inversion recovery (FLAIR), and diffusion-weighted (DWI) imaging was performed for Patients 1, 3, 4, and 5. T1 and T2 were performed for Patients 2, B,² and D.⁵

The Mann–Whitney *U* test was used for a comparison of the clinical findings and NSE values between CJD180 and sCJD. The Fisher exact probability test was used for a comparison of the positive rates of clinical symptoms, NSE, 14-3-3 protein, and PSWC.

Results. The results of the comparison between CJD180 and sCJD in each group, the MM129 group and MV129 group, are listed in table 2. The two groups had similar results, even though some were not statistically significant. CJD180 had an older onset age, longer duration from the onset to the appearance of myoclonic jerk that was less prominent compared with that of sCJD, longer duration from the onset to becoming akinetic and mute, lower value of NSE in CSF, and lower positive rate of NSE and 14-3-3 protein in CSF compared with those of sCJD. As cardinal symptoms, higher cortical dysfunctions such as aphasia and apraxia, which were not frequent symptoms in sCJD,

From the Department of Neurology (Drs. Jin, Shiga, and Itoyama), Tohoku University School of Medicine, Sendai, Department of Neurology (Dr. Shibuya), Miyagi National Hospital, Yamamoto, Department of Neurology (Dr. Chida), Kohnan Hospital, Sendai, Department of Neurology (Dr. Sato), Research Institute for Brain and Blood Vessels-Akita, Akita, Department of Neurology (Dr. Konno), Nishitaga National Hospital, Sendai, Department of Neuropathology (Dr. Koh-ura), Neurological Institute, Kyushu University Faculty of Medicine, Fukuoka, and Department of Neurological Science (Dr. Kitamoto), Tohoku University School of Medicine, Sendai, Japan.

Presented in part at the 127th annual meeting of the American Neurological Association, New York, NY, October 14, 2002.

Received April 16, 2003. Accepted in final form October 6, 2003.

Address correspondence and reprint requests to Dr. Y. Shiga, Department of Neurology, Tohoku University School of Medicine, 1-1, Seiryō-machi, Aoba-ku, Sendai 980-8574, Japan; e-mail: yshiga@em.neurol.med.tohoku.ac.jp

502 Copyright © 2004 by AAN Enterprises, Inc.

Table 1 Patients' profiles in this study: five original and an additional four reported patients

Clinical features	Original patients					Previously reported patients			
	Patient 1	Patient 2	Patient 3	Patient 4	Patient 5	Patient A ^a	Patient B ^b	Patient C ^c	Patient D ^d
Age at onset, y/sex	81/F	74/M	78/M	58/M	72/M	77/F	65/F	70/F	80/M
Duration until appearance of each clinical symptom, mo									
Myoclonic jerk	-*	5	8	10	4	6	14	9	+†
Visual or cerebellar symptom	-*	-‡	-‡	-§	-‡	-‡	-‡	-‡	-‡
Akinetic mutism	-*	12	18	-§	10	18	14	9	>18
Higher cortical dysfunction	-	-	+	+	+	-	+	+	+
Parkinsonism	-	-	+	-	-	+	-	-	-
NSE value in CSF, ng/mL	32.1	13.0	19.5	22.0	60.4	NE	NE	NE	29.9
14-3-3 protein in CSF	+	-	+	-	NE	NE	NE	NE	NE
Duration from onset to CSF study, mo	3	6	1	4	3	5	Uncertain	2	1
PSWC in EEG	-	-	-	-	-	-	-	-	-
Codon 129 in PRNP	M/V	M/M	M/V	M/V	M/M	M/V	M/M	M/M	M/V
PrP staining	NE	NE	NE	NE	NE	+	NE	+	±

Patient A was previously reported by Matsumura et al.³ Patient B was previously reported by Ishida et al.³ Patient C was previously reported by Kobayashi et al.⁴ Patient D was previously reported by Iwasaki et al.⁵

* We could not detect referring symptoms during our observation period in Patient 1 (until 15 mo after the onset). † The duration until the appearance of myoclonic jerk in Patient D is uncertain. ‡ We or the authors could not detect visual or cerebellar symptoms during the observation period. The patients' severe dementia or consciousness disturbance prevented us from making a close neurologic examination in the advanced stage.

§ We could not detect the referring symptoms during our observation period in Patient 4 (until 16 mo after the onset).

|| The presence or lack of presence as initial symptoms.

NSE = neuron-specific enolase; NE = not examined; PSWC = periodic sharp and wave complexes; PRNP = prion protein gene; M/V = methionine/valine heterozygosity at codon 129 in PRNP; M/M = methionine homozygosity at codon 129 in PRNP; PrP = prion protein.

Table 2 Comparison of clinical features between CJD180 and sCJD

Features	CJD with MM129			CJD with MV129		
	CJD180	sCJD	p value	CJD180	sCJD	p value
Age at onset, y	70.3 ± 3.9 (n = 4)	65.3 ± 11.6 (n = 116)	0.32	74.8 ± 9.5 (n = 5)	62.6 ± 10.5 (n = 5)	<0.05
Myoclonic jerk, mo*†	8.0 ± 4.5 (n = 4)	2.7 ± 2.4 (n = 113)	<0.01	9.8 ± 3.9 (n = 4)	8.2 ± 5.1 (n = 5)	0.71
Akinetic mutism, mo*‡	11.3 ± 2.2 (n = 4)	3.5 ± 2.8 (n = 113)	<0.005	17.0 ± 1.4 (n = 5)	10.4 ± 5.4 (n = 5)	<0.05
Visual symptom, %§	0.0 (n = 4)	24.0 (n = 96)	0.26	0.0 (n = 5)	20.0 (n = 5)	0.29
Cerebellar symptom, %§	0.0 (n = 4)	12.5 (n = 96)	0.45	0.0 (n = 5)	40.0 (n = 5)	0.11
Higher cortical dysfunction, %§	75.0 (n = 4)	5.2 (n = 96)	<0.0001	60.0 (n = 5)	0.0 (n = 5)	<0.05
NSE value, ng/mL	36.7 ± 33.5 (n = 2)	75.9 ± 65.7 (n = 66)		25.9 ± 6.1 (n = 4)	50.6 ± 7.9 (n = 2)	
Positive rate of NSE, %¶	50.0 (n = 2)	72.7 (n = 66)		0.0 (n = 4)	100.0 (n = 2)	
Positive rate of 14-3-3 protein, %	0.0 (n = 1)	87.7 (n = 65)		66.7 (n = 3)	100.0 (n = 2)	
PSWC in EEG, %	0.0 (n = 4)	94.0 (n = 116)	<0.0001	0.0 (n = 5)	60.0 (n = 5)	<0.05

Values are means ± SD where applicable.

* The duration until the appearance of referring symptoms.

† Patient 1 had not demonstrated myoclonic jerk 15 mo after the onset, and we accepted 15 mo for the statistical comparison. Patient D^d demonstrated myoclonic jerk, but we could not identify the duration until the appearance. Therefore, we eliminated Patient D from the statistical comparison.

‡ Patients 1 and 4 had not become akinetic and mute, and we could not identify the date when Patient D^d become akinetic and mute. Therefore, for the statistical comparison, we accepted the date when they were last confirmed not to be akinetic and mute, i.e., 15 mo for Patient 1, 16 mo for Patient 4, and 18 mo for Patient D.

§ The rate of referring symptoms as initial symptoms.

|| NSE or 14-3-3 protein in CSF.

¶ The cut-off value was 35.0 ng/mL.

CJD = Creutzfeldt-Jakob disease; sCJD = sporadic CJD; NSE = neuron-specific enolase; PSWC = periodic sharp and wave complex.

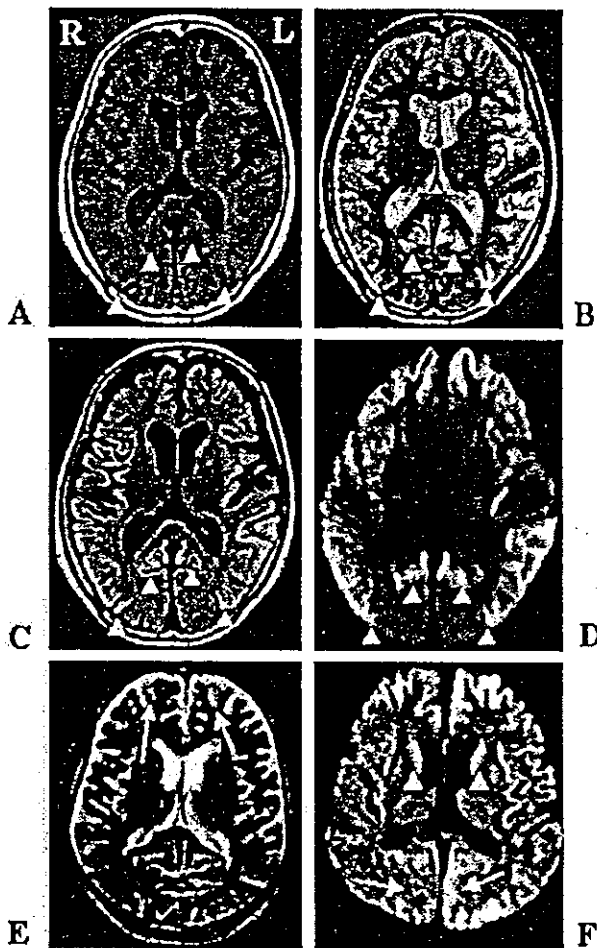


Figure. MRI of Patient 1 (A through D) and a patient with sporadic Creutzfeldt-Jakob disease (CJD) (E and F). For Patient 1 (82-year-old woman), the MRI studies were performed 4 months after the onset using 1.5 T MR unit (Magnetom Vision; Siemens, Erlangen, Germany) equipped with a conventional head coil. At this time, she demonstrated only memory disturbance and could perform her daily activities with minimal support. The wide-ranging cortical ribbon is symmetrically depicted as a low-intensity lesion by T1-weighted imaging (A) and as a high-intensity lesion by T2-weighted (B), fluid-attenuated inversion recovery (C), and diffusion-weighted (D) imaging and has a swollen appearance. The basal ganglia are not involved. Characteristically, the medial regions posterior to the parieto-occipital sulcus in the occipital lobes are not involved (arrowheads). The cerebellum was not depicted as an abnormal-intensity lesion (data not shown). For the patient with sporadic CJD with methionine homozygosity at codon 129 (70-year-old man), the MRI studies were performed 2 months after the onset using the same MR unit. At this time, he was totally bedridden and did not respond to any simple orders but opened his eyes when his name was called loudly. He showed myoclonus and startle reflex. The wide-ranging cortical ribbon including the occipital lobe (arrows) and the bilateral caudate heads (arrowheads) are depicted as a high-intensity lesion by diffusion-weighted imaging (F), although T2-weighted imaging examined at the same time demonstrates a high-intensity lesion in only the frontal lobe (arrows).

504 NEUROLOGY 62 February (1 of 2) 2004

were recognized in three of four CJD180 cases with MM129 and three of five CJD180 cases with MV129 in the very early phase. On the other hand, no CJD180 patients demonstrated visual or cerebellar symptoms, which were cardinal in sCJD. Irrespective of the polymorphism at codon 129, no CJD180 patients demonstrated PSWC in repeated EEG in their disease course.

In the MRI study, the wide range of the cortical ribbon was depicted as a low-intensity area by T1I and a high-intensity area by T2I, FLAIR, and DWI and had a swollen appearance (figure, A through D). These cortical lesions were remarkable compared with the severity of the clinical symptoms. The basal ganglia lesions were less remarkable compared with the cortical lesions. Characteristically, the medial regions, posterior to the parieto-occipital sulcus in the occipital lobes (see the figure, A through D, arrowheads), and the cerebellum were never involved in the early stage. These cortical lesions were not always symmetric in the first MRI. In sequential MRI performed in six of seven patients, these cortical lesions expanded and, in one patient,⁹ finally included the medial occipital regions. The swollen cortical lesions became atrophied in the advanced stage, but not as severe as compared with the brain atrophy of sCJD.

Discussion. V180I is recognized as a causative point mutation based on the result that V180I was detected only in CJD patients but not in 200 normal Japanese persons.⁹ The World Health Organization also lists CJD180 as familial CJD.¹

We clarified the clinical and laboratory characteristics of CJD180 by comparing them with those of sCJD. CJD180 showed 1) older onset age; 2) slower progression of the disease; 3) unique clinical symptoms such as frequent higher cortical dysfunction, which was less frequent in sCJD, no visual or cerebellar symptoms, which were important for sCJD, and less remarkable myoclonic jerk compared with the generalized one in sCJD; 4) a lower positive rate of brain-specific proteins such as NSE and 14-3-3 protein in CSF; and 5) no PSWC in EEG throughout the disease course. These features render it difficult to make a premortem diagnosis of CJD180 based on the clinical features without a PRNP analysis.

In our experience, the most useful test leading to the genetic analysis was MRI. The abnormal lesions in MRI of sCJD are varied,¹⁰ but those of CJD180 are rather uniform. In accordance with the absence of visual or cerebellar symptoms in the early stage, the medial occipital lobes posterior to the parieto-occipital sulcus or the cerebellum were never involved until the terminal stage. A disproportionately remarkable cortical lesion compared with the severity of the clinical symptoms and less remarkable basal ganglia lesion must be recognized as characteristic MRI findings. At present, we must recognize an uncommon variant of familial CJD that might have been misdiagnosed. Therefore, we recommend MRI study including DWI for patients with progressive dementia. Then, we should perform a PRNP analysis

in all patients with progressive dementia and characteristic MRI abnormalities.

Parkinsonism, which was a rare symptom in sCJD, occurred in two of five CJD180 cases with MV129 in the very early stage. It is important to discriminate among neurodegenerative disorders presenting dementia with parkinsonism from CJD180. MRI can provide us useful information.

CJD180 is clearly associated with a point mutation of *PRNP* but appears as if it were a sporadic neurodegenerative disorder. We may misdiagnose such cases without a genetic analysis because of the difference in the clinical features from what we usually consider the "CJD characteristic" clinical features. Characteristic MRI findings can lead us to an accurate premortem diagnosis.

Acknowledgment

The authors thank Drs. Nobuhito Seno, Takafumi Hasegawa, Michiko Matsuzaki, Masahiro Asano, Atsushi Takeda, and Nobuyuki Sato for clinical support; Drs. Shuichi Higano and Shoki Takahashi for performing the MRI study; and Mr. Brent Bell for reading the manuscript.

References

1. Zeidler M, Gibbs CJ Jr, Meslin F. WHO manual for strengthening diagnosis and surveillance of Creutzfeldt-Jakob disease. Geneva: World Health Organization, 1998.
2. Matsumura T, Kojima S, Kuroiwa Y, et al. An autopsy-verified case of Creutzfeldt-Jakob disease with codon 129 polymorphism and codon 180 point mutation. *Clin Neurol* 1995;35:282-285.
3. Ishida S, Sugino M, Koizumi N, et al. Serial MRI in early Creutzfeldt-Jakob disease with a point mutation of prion protein at codon 180. *Neuroradiology* 1995;37:531-534.
4. Kobayashi S, Ohuchi T, Maki T, et al. A case of probable Creutzfeldt-Jakob disease with a point mutation of prion protein gene codon 180 and atypical MRI findings. *Clin Neurol* 1997;37:671-674.
5. Iwasaki Y, Sone M, Kato T, et al. Clinicopathological characteristics of Creutzfeldt-Jakob disease with a PrP V180I mutation and M129V polymorphism on different alleles. *Clin Neurol* 1999;39:800-806.
6. Hitoshi S, Nagura H, Yamanouchi H, et al. Double mutations at codon 180 and codon 232 of the *PRNP* gene in an apparently sporadic case of Creutzfeldt-Jakob disease. *J Neurol Sci* 1993;120:208-212.
7. Nakamura Y, Watanabe M, Sato T, et al. Results of Creutzfeldt-Jakob disease surveillance in Japan. In: Hizusawa H, ed. Annual report of the Prion Disease and Slow Virus Infection Research Committee, The Ministry of Health, Labour and Welfare. 2003:26-29.
8. Aksamit AJ Jr, Preissner CM, Homburger HA. Quantitation of 14-3-3 and neuron-specific enolase proteins in CSF in Creutzfeldt-Jakob disease. *Neurology* 2001;57:728-730.
9. Kitamoto T, Ohta M, Doh-ura K, et al. Novel missense variants of prion protein in Creutzfeldt-Jakob disease or Gerstmann-Sträussler syndrome. *Biochem Biophys Res Commun* 1993;191:709-714.
10. Murata T, Shiga Y, Higano S, et al. Conspicuity and evolution of lesions in Creutzfeldt-Jakob disease at diffusion-weighted imaging. *AJNR Am J Neuroradiol* 2002;23:1164-1172.

Quinoline Derivatives Are Therapeutic Candidates for Transmissible Spongiform Encephalopathies

Ikuko Murakami-Kubo,^{1,2*} Katsumi Doh-ura,^{1*} Kensuke Ishikawa,¹ Satoshi Kawatake,^{1†}
Kensuke Sasaki,¹ Jun-ichi Kira,² Shigeru Ohta,³ and Toru Iwaki¹

Departments of Neuropathology¹ and Neurology,² Graduate School of Medical Sciences, Kyushu University, Fukuoka 812-8582, and Department of Graduate School of Biomedical Science, Hiroshima University, Hiroshima 734-8551,³ Japan

Received 2 June 2003/Accepted 8 October 2003

We previously reported that quinacrine inhibited the formation of an abnormal prion protein (PrPres), a key molecule in the pathogenesis of transmissible spongiform encephalopathy, or prion disease, in scrapie-infected neuroblastoma cells. To elucidate the structural aspects of its inhibiting action, various chemicals with a quinoline ring were screened in the present study. Assays of the scrapie-infected neuroblastoma cells revealed that chemicals with a side chain containing a quinuclidine ring at the 4 position of a quinoline ring (represented by quinine) inhibited the PrPres formation at a 50% inhibitory dose ranging from 10^{-1} to 10^1 μ M. On the other hand, chemicals with a side chain at the 2 position of a quinoline ring (represented by 2,2'-biquinoline) more effectively inhibited the PrPres formation at a 50% inhibitory dose ranging from 10^{-3} to 10^{-1} μ M. A metabolic labeling study revealed that the action of quinine or biquinoline was not due to any alteration in the biosynthesis or turnover of normal prion protein, whereas surface plasmon resonance analysis showed a strong binding affinity of biquinoline with a recombinant prion protein. *In vivo* studies revealed that 4-week intraventricular infusion of quinine or biquinoline was effective in prolonging the incubation period in experimental mouse models of intracerebral infection. The findings suggest that quinoline derivatives with a nitrogen-containing side chain have the potential of both inhibiting PrPres formation *in vitro* and prolonging the incubation period of infected animals. These chemicals are new candidates for therapeutic drugs for use in the treatment of transmissible spongiform encephalopathies.

Transmissible spongiform encephalopathies (TSEs), or prion diseases, are a group of fatal neurodegenerative disorders that include Creutzfeldt-Jakob disease and Gerstmann-Sträussler-Scheinker disease (GSS) in humans and scrapie, bovine spongiform encephalopathy, and chronic wasting disease in animals. These disorders are characterized by the accumulation of an abnormal isoform of prion protein (PrPres), which is high in beta-sheet content and resistant to digestion with proteases (15). Recent outbreaks in younger people of acquired forms of human TSEs, such as variant Creutzfeldt-Jakob disease (19) and iatrogenic Creutzfeldt-Jakob disease with cadaveric growth hormone or dura graft (4), are prompting the development of therapeutic interventions as well as early diagnostics.

One possible therapeutic strategy is to inhibit PrPres formation in the infected host. Doh-ura et al. first reported that cysteine protease inhibitors and lysosomotropic agents inhibited PrPres formation in scrapie-infected neuroblastoma (ScNB) cells and that among them, quinacrine was one of the most

potent inhibitors (8). Another research group has also reported that quinacrine and its related tricyclic compounds are effective in inhibiting PrPres formation (11). Quinacrine is a synthesized chemical which has a quinoline ring in its structure. It is used as a substitute for quinine in the treatment of malaria. Accordingly, in this study we chose to focus on the quinoline derivatives to examine the structure-activity relationship involved in inhibiting PrPres formation as well as in prolonging the incubation time of infected animals.

MATERIALS AND METHODS

Chemicals and ScNB cells. Chemicals were purchased from Sigma, Maybridge (Cornwall, United Kingdom), Peakdale (Derbyshire, United Kingdom), Specs (Rijswijk, The Netherlands), and Bionet (Cornwall, United Kingdom) and were dissolved in 100% dimethyl sulfoxide (DMSO) or 96% ethanol just before use. ScNB cells (16) were grown in six-well culture plates in Opti-MEM (Invitrogen) supplemented with 10% fetal bovine serum. Chemicals at various concentrations were added to the medium when 1/20 of the confluent cells were passed. The final concentration of either DMSO or ethanol in the medium was less than 0.2%. The cultures were allowed to grow to confluence for 4 days.

Western blot analysis. PrPres was analyzed as described previously (5) with slight modification. Briefly, the cells in confluency were rinsed with phosphate-buffered saline (PBS) and lysed with lysis buffer (0.5% sodium deoxycholate, 0.5% Nonidet P-40, PBS). After low-speed centrifugation, the supernatant was treated with 10 μ g of proteinase K/ml for 30 min at 37°C. Digestion was stopped with 0.5 mM phenylmethylsulfonyl fluoride, and the supernatant was centrifuged at 100,000 \times g for 30 min at 4°C. Pellets were resuspended in 30 μ l of the sample buffer by sonication. After being boiled, the sample was separated by electrophoresis on a Tris-glycine-sodium dodecyl sulfate-15% polyacrylamide gel electrophoresis (SDS-PAGE) and then electroblotted onto a polyvinylidene difluoride membrane (Millipore). The membrane was incubated with PrP-2B, an anti-PrP polyclonal antibody, against a mouse-hamster PrP fragment (amino acids 89 to 103) and then with an alkaline phosphatase-conjugated goat anti-

* Corresponding author. Mailing address for Ikuko Murakami-Kubo: Department of Neuropathology, Graduate School of Medical Sciences, Kyushu University, 3-1-1 Maidashi, Higashi-ku, Fukuoka 812-8582, Japan. Phone: 81-92-642-5537. Fax: 81-92-642-5540. E-mail: i-muraka@np.med.kyushu-u.ac.jp. Mailing address for Katsumi Doh-ura: Department of Prion Research, Tohoku University Graduate School of Medicine, 2-1 Seiryō-cho, Aoba-ku, Sendai 980-8575, Japan. Phone: 81-22-717-8232. Fax: 81-22-717-8148. E-mail: doh-ura@mail.tains.tohoku.ac.jp.

† Present address: Department of Prion Research, Tohoku University Graduate School of Medicine, Sendai 980-8575, Japan.

rabbit antibody (Promega). Signals were visualized with CDP-Star detection reagent (Amersham) and were densitometrically analyzed. Either the concentration of a chemical giving 50% inhibition of PrPres formation relative to the control 50% inhibitory concentration (IC_{50}) or the maximal concentration of a chemical that does not affect the rate of cell growth to confluence (TC) was estimated from more than three independent experiments.

Metabolic labeling study. Metabolic labeling of prion protein was performed as described previously (5). Briefly, subconfluent ScNB cells in 25-cm² flasks were rinsed three times with PBS and preincubated at 37°C in 1.5 ml of methionine-free minimal essential medium with 1% dialyzed fetal bovine serum and 1 μ M quinine or 2,2'-biquinoline. After 60 min of preincubation, 125 μ Ci of ³⁵S-labeled methionine (Amersham) was added to each flask and incubated for 60 min. Then 10 ml of chase medium with 1 μ M quinine or biquinoline was added, and the incubation was continued for 18 min, 2 h, or 8 h. Cells were rinsed three times with PBS and lysed with lysis buffer. After low-speed centrifugation, an aliquot of the supernatant was electrophoresed for total protein analysis; the remainder was used for immunoprecipitation of total prion protein. For the detection of cell surface phosphatidylinositol-anchored prion protein, cells were incubated for 30 min in the chase medium with 1 μ M quinine or biquinoline after pulse labeling, rinsed three times with PBS, and then incubated with 1.33 U of phosphatidylinositol-specific phospholipase C (PIPLC)/ml in PBS at 37°C for 60 min. The soup was used for immunoprecipitation of cell-surface prion protein. Immunoprecipitation was performed with a PrP-2B antibody after whole proteins in the soup were precipitated with methanol and resuspended in detergent-lipid-protein complex solution.

Surface plasmon resonance sensorgram study. Interaction between prion protein and a chemical was analyzed using a BIAcore X systems. A recombinant murine prion protein fragment (amino acids 121 to 231) (PrP121-231) was immobilized on a sensor chip (CM5) according to the manufacturer's instructions. Each chemical was injected at a 100 μ M concentration in running buffer (2.5% DMSO in PBS) for 1 min at a flow rate of 20 μ l/min; then running buffer without a chemical was injected for 1 min at the same flow rate. Data were corrected by using a blank sensor chip as a control.

In vivo study. In vivo evaluation of the effectiveness of a chemical at prolonging the incubation times in infected animals was performed by using a mouse model of Tg7 (14, 17) or Tg20 (10), both of which have substantially shorter incubation periods than wild mice. Briefly, a 20- μ l aliquot of 1% 263K pathogen homogenate for Tg7 mice, or the same amount of aliquot of 1% Rocky Mountain Laboratory (RML) pathogen homogenate or Fukuoka-1 pathogen homogenate for Tg20 mice, was inoculated into the right parietal portion of the brain. A 4-week continuous intraventricular infusion of vehicle alone (25% DMSO) or of a chemical dissolved in 25% DMSO was initiated at day 10 or 35 in Tg7 mice or at day 14 or 49 in Tg20 mice by using an Alzet osmotic pump equipped with a brain infusion kit (Durect, Cupertino, Calif.). An intraventricular infusion cannula from the brain infusion kit was fitted into the left frontal portion of the brain.

The infusion initiation date was selected at an early stage of the infection (day 10 or 14), or at a late stage (day 35 or 49), when abnormal PrP deposition in the brain definitely appeared in the 263K-infected Tg7 or RML-infected Tg20 mice. However, day 49 postinoculation in the Fukuoka-1-infected Tg20 mice was not exactly at a late stage of the infection, and no information on when abnormal PrP deposition appeared in this model was available.

In some experiments, intraperitoneal administration of a chemical was provided by a single injection once a day for 5 days per week from day 10 or day 35 postintracerebral inoculation until death. The incubation period during which the animals were observed every day lasted from the time of intracerebral infection until the time of death. Five male mice (each weighing about 30 g) per group were used in the experiments. Animal handling and killing were in accordance with national prescribed guidelines, with ethical approval for the study granted by the Animal Experiment Committee of Kyushu University.

Mice which died within a few days due to operational procedures were excepted from the statistical analysis after pathological confirmation. Doses of less than 8 nmol of quinine/day were examined, because toxicity shortened life span at doses beyond 8 nmol/day. Biquinoline was examined at doses of less than 16 nmol/day, which provided no toxicity yet solubility in 25% DMSO.

Immunohistochemistry. An indirect immunoperoxidase method was applied as described previously (9) with slight modification. Briefly, brains were obtained postmortem and fixed in 10% buffered formalin for several weeks. The tissue was immersed in 98% formic acid for 1 h to reduce infectivity and then embedded in paraffin. The samples were cut into 5- μ m-thick sections, and then the sections were deparaffinized in xylene and hydrated using an ethanol gradient. The endogenous peroxidase activity was blocked with 0.3% H₂O₂ in absolute methanol for 30 min at room temperature. After being rinsed with tap water, the

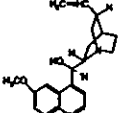
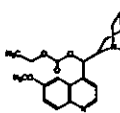
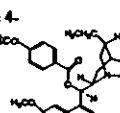
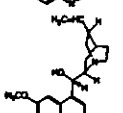
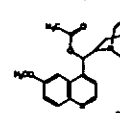
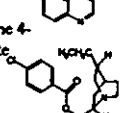
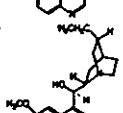
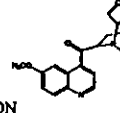
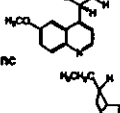
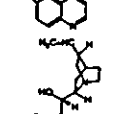
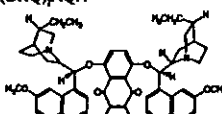
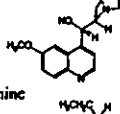
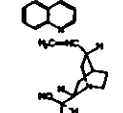
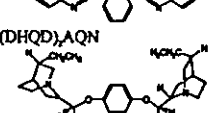
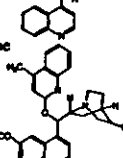
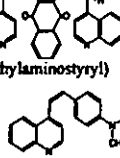
sections were treated with a hydrolytic autoclave (1 mM or 1.5 mM HCl, 121°C, 10 min) and washed in 50 mM Tris-HCl, pH 7.6, before being incubated with PrP-C polyclonal antibody (Immuno-Biological Laboratories, Gunma, Japan) (1:200) at 4°C overnight. The sections were then incubated with a horseradish peroxidase-conjugated secondary antibody (Vector Laboratories, Burlingame, Calif.) (1:200). The color reaction product was developed with 3,3'-diaminobenzidine tetrahydrochloride solution, and the sections were then counterstained with hematoxylin.

RESULTS

Screening of chemicals in vitro. Clinically available drugs with a quinoline ring and their related chemicals were first screened for the inhibition of PrPres formation in ScNB cells. The antimalarial drug quinine and its related chemicals (such as quinidine, hydroquinine, cinchonine, cinchonidine, and hydroquinidine 4-methyl-2-quinolyl ether) were found to be effective (Table 1, left column). The IC_{50} doses of these chemicals ranged from 3 to 18 μ M, and the effective dose range between the IC_{50} and the TC was relatively narrow. Hydroquinidine 4-methyl-2-quinolyl ether, which has two quinoline rings, was slightly more effective than the chemicals with only one quinoline ring. Quinine-related chemicals with a carbonyl base located between a quinoline ring and a quinuclidine ring, such as MQAC (cinchonon-9-ol, 6'-methoxy-ethylcarbonate), MQAA (cinchonon-9-ol, 6'-methoxy-acetate), and MAM [(6-ethynyl-1-azabicyclo[2.2.2]oct-2yl) (6-methoxy-4-quinolinyl) methanone], were more effective, and their IC_{50} dose ranges were 0.45 to 0.9 μ M (Table 1, middle column). Chemicals with either the motif of quinine or that of quinidine on each lateral side of anthraquinone, (DHQ)₂AQN (hydroquinine anthraquinone-1,4-diyl diether) and (DHQD)₂AQN (hydroquinidine anthraquinone-1,4-diyl diether), were much more effective than those with only one motif, and their IC_{50} doses were 0.04 and 0.01 μ M, respectively. A chemical with a 4-dimethylamino-styryl moiety was also very effective; and its IC_{50} was 0.012 μ M. Except for this chemical, all of the effective chemicals shared a common structure composed of a quinoline ring plus a relative large side chain containing a quinuclidine ring at the 4 position of the quinoline ring. The chemicals listed in the right column of Table 1 also had this common structure, but they showed toxicity at a lower dose and were not effective within a nontoxic dose range.

Other quinoline chemicals unrelated to quinine were also screened. Chemicals with a side chain at the 2 position of a quinoline ring, such as 2,2'-biquinoline, inhibited PrPres formation at 0.003 μ M, the minimum IC_{50} dose (Fig. 1A), and this effectiveness was reduced by the replacement of the quinoline ring by a pyridine ring or a naphthyridine ring (Table 2, left column). The addition of a carboxyl moiety to both the 4 position and the 4' position of the quinoline ring abolished the inhibiting activity of biquinoline (Table 2, right column, top). QCQH (8-hydroxy-8-quinolinylhydrazone-2-quinolinecarboxaldehyde) and PCQH (2-quinolinylhydrazone-2-pyridinecarboxaldehyde) were also very effective in inhibiting PrPres formation at an IC_{50} dose of 0.0075 and 0.004 μ M, respectively. They shared a common structure with biquinoline respecting the arrangement of nitrogen atoms. DMEDAPQ (*N,N*-dimethyl-*N'*-[2-(4-pyridinyl)-4-quinolinyl]-1,2-ethanediamine) a chemical with a nitrogen-containing side chain at both the 2 position and the 4 position of a quinoline ring (thereby resem-

TABLE 1. Structure-activity relationship of quinine analogues on PrPres inhibition

Effective				Ineffective							
Chemical	Structure	IC ₅₀ (μM) ^a	TC (μM) ^b	Chemical	Structure	IC ₅₀ (μM) ^a	TC (μM) ^b				
Quinine		6	50	MQAC		0.45	25	Hydroquinine 4-chlorobenzoate		-	5
Quinidine		3	>50	MQAA		0.5	>50	Hydroquinidine 4-chlorobenzoate		-	>5
Hydroquinine		12.5	50	MAM		0.9	>50	Hydroquinidine		-	2.5
Cinchonine		6	25	(DHQ) ₂ AQN		0.04	5	Hydrocinchonine		-	25
Cinchonidine		18	50	(DHQD) ₂ AQN		0.01	5				
Hydroquinidine 4-methyl-2-quinoly ether		3.5	>5	4-(4-Dimethylaminostyryl) quinoline		0.012	10				

^a IC₅₀, approximate concentration of a chemical giving 50% inhibition of PrPres formation relative to the control.
^b TC, approximate maximal concentration of a chemical that does not affect the rate of cell growth to confluence.

bling quinine rather than biquinoline in terms of the arrangement of nitrogen atoms), was less effective than biquinoline, and its IC₅₀ dose was 0.5 μM.

Chemicals containing a quinoline ring without a large side chain were also examined. They included quinoline hydrochloride, 8-hydroxyquinoline, 2,8-quinolinediol, 8-acetoxyquinoline, and CHIQ (5-chloro-7-iodo-8-quinolinol). All of them, with the exception of 2,8-quinolinediol, were ineffective at inhibiting PrPres within a nontoxic dose range (Table 2, right column). Quinolinediol showed an IC₅₀ dose of 8 μM, which was much higher than those of other chemicals with a side chain at the 2 position of a quinoline ring (Table 2, left column, bottom).

Mechanism of inhibition of PrPres formation. Because quinine and biquinoline represented the effective chemicals found here, we focused on these chemicals and studied the mechanism behind their action. After ScNB cells had been treated with different concentrations of quinine or biquinoline for 4 days and then left without treatment for an additional 10 or 17 days, PrPres signals did not reappear even 17 days after discontinuation of the chemical treatment (Fig. 1B [for biquinoline] and data not shown [for quinine]). Thus, treatment with the chemicals permanently cured the cells of the accumulation of PrPres.

Because phospholipase-sensitive cell surface PrP (PrP^{sen}) is

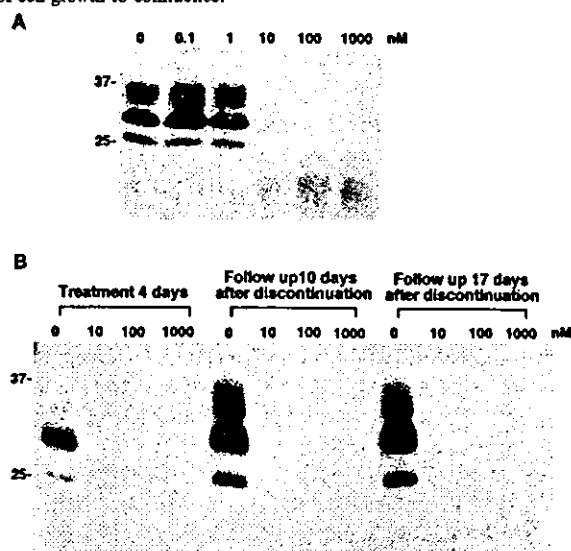

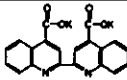
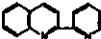
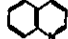

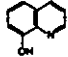
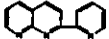
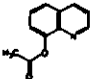
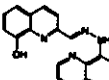
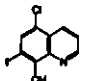
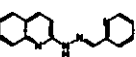
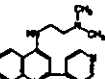
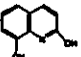


FIG. 1. Inhibition of PrPres accumulation in ScNB cells grown with 2,2'-biquinoline (A) and lack of restoration of PrPres formation in ScNB cells treated once with biquinoline (B). (A) Biquinoline was added at designated concentrations to the medium when the cells were passed, and the culture was allowed to grow to confluence. Then, PrPres in the cells was analyzed by immunoblotting. (B) ScNB cells were treated with 10, 100, or 1,000 nM biquinoline for 4 days. The medium was replaced by fresh medium, and the cells were left without treatment for an additional 10 or 17 days. Then PrPres levels were assayed. Molecular size markers (in kilodaltons) are indicated.

TABLE 2. Structure-activity relationship of biquinoline analogues on PrPres inhibition

Effective				Ineffective			
Chemical	Structure	IC ₅₀ (μM) ^a	TC (μM) ^b	Chemical	Structure	IC ₅₀ (μM) ^a	TC (μM) ^b
2,2'-Biquinoline		0.003	>10	BQDA		-	>100
2-(2-Pyridinyl)quinoline		0.11	50	Quinoline hydrochloride		-	>25
2,2'-Bi(1,8-naphthyridine)		38	>100	8-Hydroxyquinoline		-	1
2-(2-Pyridinyl)-1,8-naphthyridine		12	200	8-Acetoxyquinoline		-	2.5
QCQH		0.0075	2.5	CHIQ		-	>5
PCQH		0.004	1				
DMEDAPQ		0.5	50				
2,8-Quinolinediol		8	>50				

^a IC₅₀, approximate concentration of a chemical giving 50% inhibition of PrPres formation relative to the control.

^b TC, approximate maximal concentration of a chemical that does not affect the rate of cell growth to confluence.

the precursor of PrPres, it is possible that the inhibition of PrPres accumulation by these chemicals was due to an indirect effect on PrPsen metabolism or turnover. However, biquinoline showed no effects on the metabolic labeling of cellular proteins or on the biosynthesis and turnover of PrPsen (Fig. 2A, B, and C).

Surface plasmon resonance analysis showed that the interaction of biquinoline with recombinant PrP121-231 occurred very slowly and failed to reach saturation even after 1 min. During the dissociation phase, furthermore, complete dissociation did not occur (Fig. 2D). On the other hand, the interaction of quinine or quinacrine occurred very quickly, reaching saturation within several seconds, and dissociation was completely over within seconds.

From observations of the structure of the effective chemicals, it was predicted that they might exert their inhibiting action through some mechanism which involved chelating metals. Thus, quinine and biquinoline were preincubated (before being added to the ScNB culture medium) with an equivalent dose of, a 10-times-higher dose of, or a 100-times-higher dose of various metal ions, including copper, zinc, manganese, iron, cobalt, and aluminum ions. The results showed no change in the inhibiting activities of the chemicals (data not shown).

In vivo study. To examine whether these chemicals could be effective in improving the prognosis in vivo, quinine or biquinoline was continuously administered intraventricularly in animal

models which had been intracerebrally infected with three different TSE pathogen strains, comprising 263K scrapie agent, RML scrapie agent, and Fukuoka-1 GSS agent. Quinine administration from an early stage of infection prolonged the incubation period by 13.6% (days 47 to 53.4) at 0.64 nmol/day in 263K-infected mice (Fig. 3A), by 10.8% (days 68.6 to 76) at 1.6 nmol/day in RML-infected mice (Fig. 3B), and by 12.8% (days 104.2 to 117.5) at 0.64 nmol/day in Fukuoka-1-infected mice (Fig. 3C). The effect of quinine administration from a late stage of infection was clearly demonstrated in 263K-infected mice, resulting in 36% (days 47 to 63) prolongation of the incubation period at 1.6 nmol/day (Fig. 3A), with some of the RML-infected mice displaying a tendency to survive much longer than the control at 0.64 nmol/day (Fig. 3B). On the other hand, the effect of biquinoline administration was examined only in 263K-infected mice; it demonstrated 10.8% (days 49 to 54.3) prolongation of the incubation period in the group receiving 1.6 nmol/day at an early stage of infection, but no significant effects were observed in the groups which received it at a late stage (Fig. 3D). Intraperitoneal administration of biquinoline was also performed in 263K-infected mice, and this resulted in 7.7% (days 49 to 52.8) prolongation of the incubation period in the group receiving 0.39 mmol/day from an early stage of infection.

Postmortem histopathological examination of the brains treated with quinine or biquinoline was performed to see

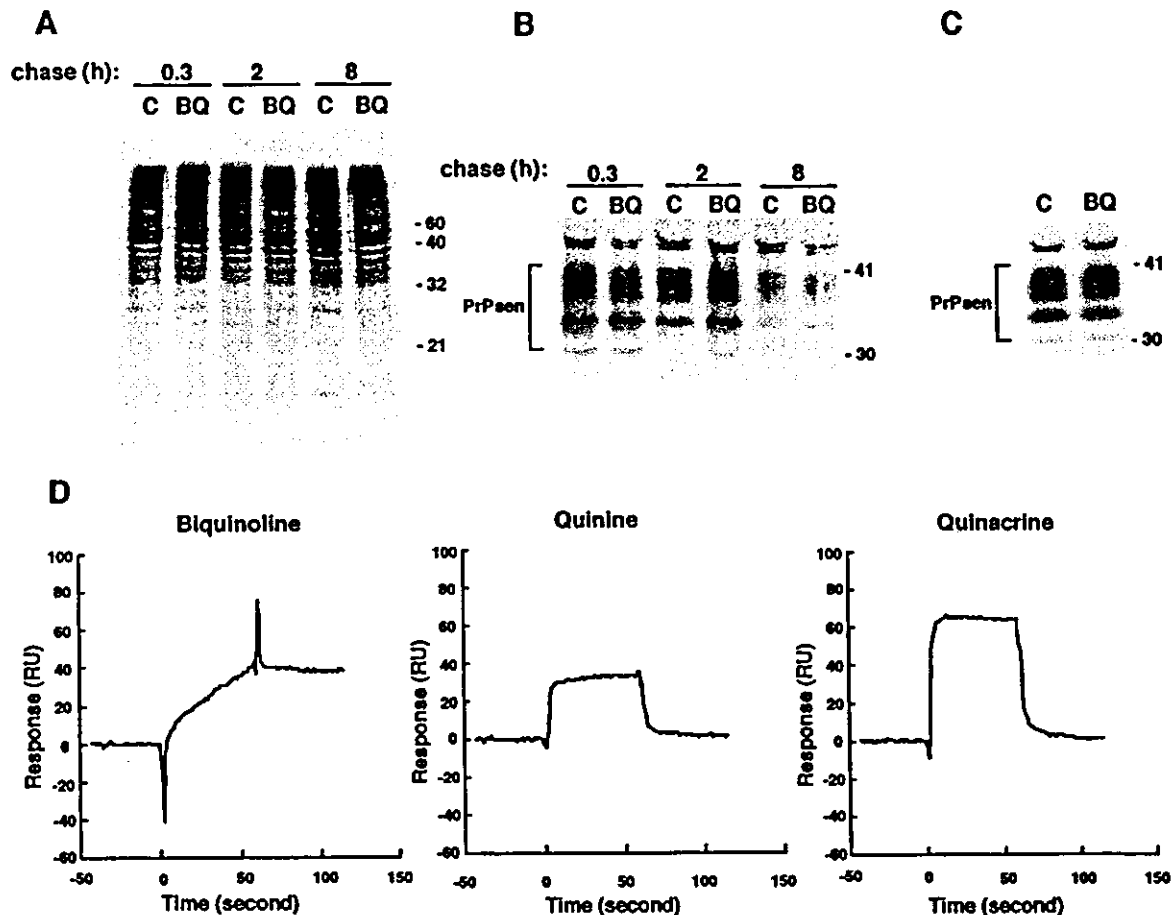


FIG. 2. Lack of effect of the presence of biquinoline on the metabolic labeling of total protein (A), total PrPsen (B), and PIPLC-sensitive, cell surface PrPsen (C). (D) Direct interaction of biquinoline with recombinant PrP121-231 analyzed using a surface plasmon resonance sensorgram. (A) Control ScNB cells (lanes C) and biquinoline-treated cells (lanes BQ) were pulse labeled and then incubated in chase medium for the indicated chase time. The total lysate proteins were methanol precipitated from the detergent lysates of the cells and analyzed by SDS-PAGE. Equal flask equivalents were loaded onto all lanes in each panel. Molecular size markers (in kilodaltons) are indicated. (B) PrPsen was isolated from the total lysate proteins by immunoprecipitation and analyzed by SDS-PAGE. (C) PrPsen was immunoprecipitated from the cell soup treated with PIPLC. Biquinoline at 1 μ M was included in all media, starting with the preincubation, except in the case of the control cells. (D) Interaction between a PrP121-231 fragment and a chemical was analyzed using a BIAcore system. A recombinant murine PrP121-231 fragment was immobilized on a CM5 sensor chip; biquinoline, quinine, or quinacrine (at 100 μ M in buffer solution) was injected for 1 min at a flow rate of 20 μ l/min for the association, and then the buffer solution without a chemical was injected at the same flow rate for the dissociation.

whether there was any modification in abnormal PrP deposition patterns following treatment. Those mice with prolonged incubation periods had a tendency to show less PrP deposition in the white matter between the cerebral cortex and the hippocampus of the brain hemisphere implanted with an intraventricular cannula, although they showed no apparent alteration in PrP deposition patterns in the bilateral thalamus or hypothalamus (Fig. 4).

DISCUSSION

In the studies reported here, we were able to identify quinoline derivatives that inhibited PrPres accumulation in ScNB cells. The commonly shared structure in these chemicals was a quinoline ring bound at its 2 or 4 position with a side chain containing a nitrogen atom, which was located at a particular distance from a nitrogen atom in the ring. Chemicals with a

side chain at the 2 position of a quinoline ring were more effective than those with a side chain at the 4 position. Replacement of a quinoline ring with a pyridine ring or a naphthyridine ring resulted in a weaker inhibiting activity, while modification of biquinoline by a moiety that caused less flexibility in the hinge portion between the quinoline rings completely suppressed the inhibiting activity. These findings suggest that a certain proper alignment of two nitrogens, one in a quinoline ring and the other in a side chain, might be important with regard to inhibiting activity.

As for the inhibiting mechanism of these chemicals, the representative chemicals, quinine and biquinoline, demonstrated no alteration either in the protein biosynthesis in general or in the metabolic labeling and turnover of PrPsen in particular. However, biquinoline showed a very strong binding affinity with recombinant PrP121-231 in the BIAcore study. Thus, some of the chemicals, including biquinoline, may inhibit

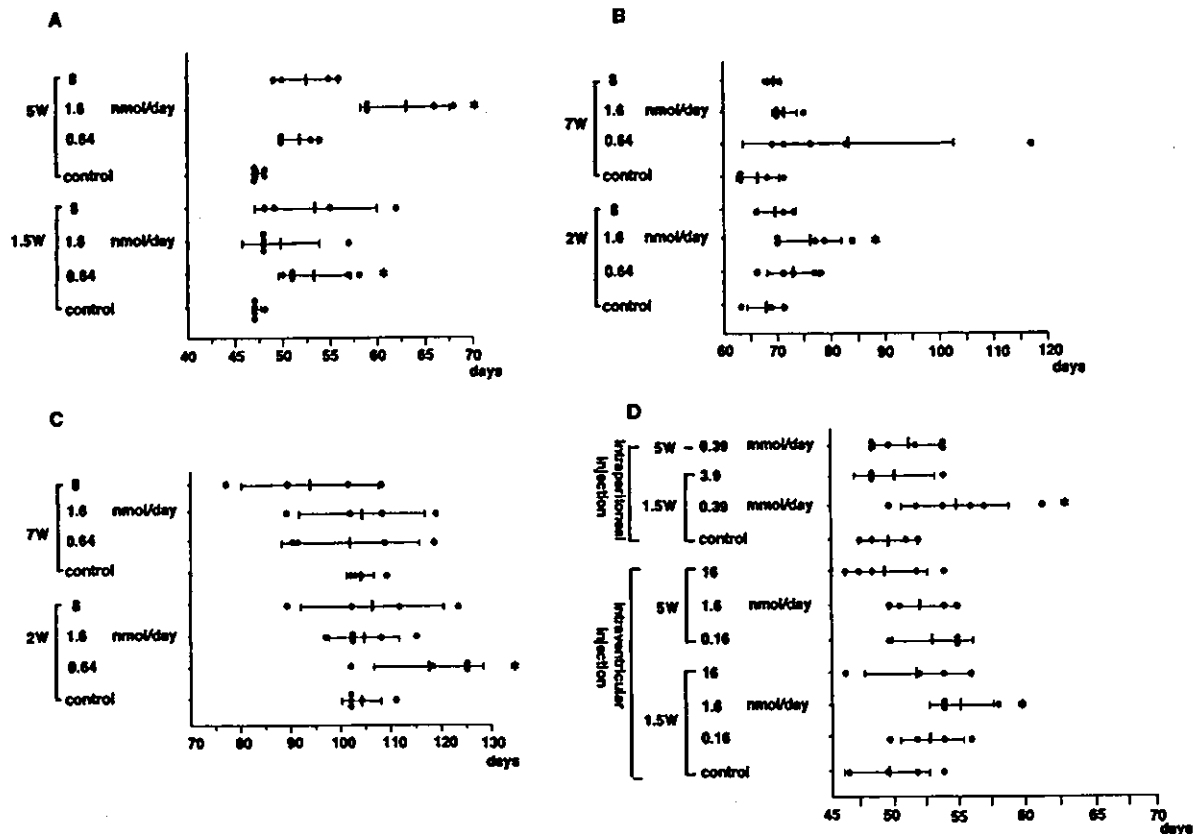


FIG. 3. Prolongation of incubation times in intracerebrally TSE-infected mice treated with quinine or biquinoline. (A) Tg7 mice infected with 263K agent strain and intraventricularly treated with quinine; (B) Tg20 mice infected with RML agent strain and intraventricularly treated with quinine; (C) Tg20 mice infected with Fukuoka-1 agent strain and intraventricularly treated with quinine; (D) Tg7 mice infected with 263K agent strain and intraperitoneally or intraventricularly treated with biquinoline. A 4-week continuous intraventricular infusion of a chemical was initiated by using an osmotic pump at day 10 (1.5W) or day 35 (5W) post-intracerebral inoculation in Tg7 mice or at day 14 (2W) or day 49 (7W) in Tg20 mice. For intraperitoneal treatment, injection of a chemical in Tg7 mice was performed intraperitoneally once a day for 5 days per week from day 10 (1.5W) or day 35 (5W) until the death of the mouse. Each closed circle represents the incubation time of an individual mouse. Each solid line and bar represent the average and standard deviation of the incubation times of each group. The star indicates groups with $P < 0.05$ compared to the results seen with the vehicle control. Each of the experiments was performed independently using different lots of the pathogen homogenate; thus, there was some variation in the data shown in panels A and D even for the same vehicle control.

the conversion of PrPsen to PrPres through direct interaction with PrPsen molecules. Since biquinoline (IC_{50} dose, 0.003 μ M) was much more effective than quinine (3 μ M) or quinacrine (at a concentration of 0.4 μ M [8] or 0.3 μ M [11]) in ScNB cells, the binding affinity of the PrP fragment (which was much stronger with biquinoline than with quinine or quinacrine) would appear to be clearly correlated with the inhibiting activity of PrPres formation in vitro. The potential binding site(s) of these chemicals in PrPsen molecules remains to be determined.

On the other hand, the involvement of chelating metal(s) in their inhibiting activity (as determined on the basis of the structure of the chemicals which were found to be effective in this study) was predicted. PrPsen is known to bind copper at its N-terminal octameric repeat region (3, 13, 18), and it is suggested that interaction between PrPres and copper stabilizes PrPres conformation (12). Manganese also binds PrP molecules instead of copper and increases proteinase K resistance and beta-sheet content (2). However, our observation suggests

that the chelating mechanism seems unlikely to be involved in the inhibiting action of the chemicals found here.

Among the chemicals tested here, CHIQ is an antibiotic (called clioquinol) and a Cu/Zn-selective chelator known to be effective in decreasing beta-amyloid deposits in Alzheimer's disease (6). However, in this study, CHIQ and its related compounds, quinoline hydrochloride, 8-hydroxyquinoline, and 8-acetoxyquinoline, did not inhibit PrPres formation in ScNB cells. These findings also suggest that chelating drugs which are effective in inhibiting beta-amyloid formation are not necessarily effective at inhibiting PrPres formation.

The in vivo study revealed that the chemicals with a quinoline ring were effective not only in inhibiting PrPres formation in vitro but also in prolonging incubation times of intracerebrally infected animals. The greatest effectiveness was obtained by intraventricular administration of quinine at 1.6 nmol/day, which prolonged the incubation time by 36% in 263K-infected mice (compared to the results seen with the control) when initiated at a late stage of infection. Quinine was also effective

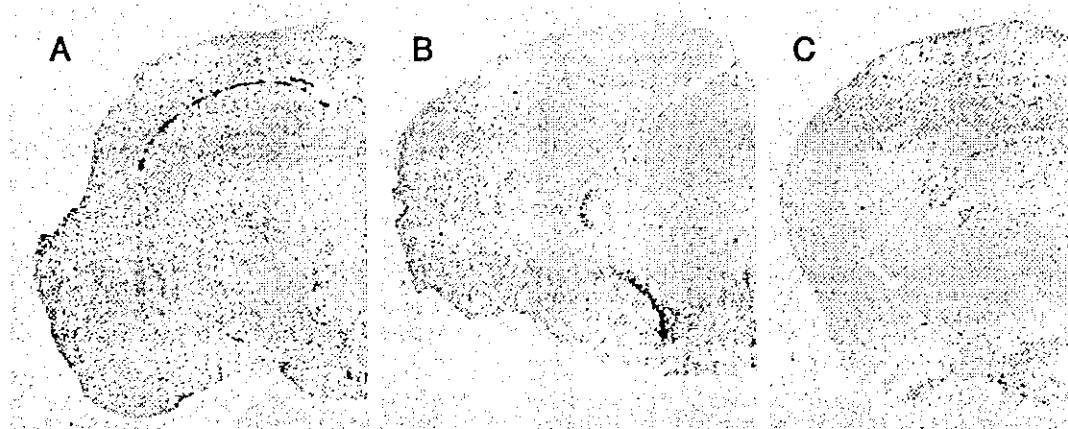


FIG. 4. Effects of intraventricular treatment with quinine or biquinoline on abnormal PrP deposition in the brain of intracerebrally 263K-infected Tg7 mice. The results for brain treated from day 10 postinfection for 4 weeks with vehicle (25% DMSO) alone (A), 0.64 nmol of quinine/day (B), or 1.6 nmol of biquinoline/day (C) are shown. Immunohistochemistry for abnormal PrP deposition was performed in the brains obtained postmortem from the longest-surviving members in each group, and representative examples of the brain hemisphere at the chemical injection side are shown.

in prolonging incubation times of the mice inoculated with different pathogen strains such as RML scrapie agent and Fukuoka-1 GSS agent. These findings indicate that application of quinine, an antimalarial drug, to humans infected with other TSE agents could be judicious.

Recently two research groups have reported that quinacrine is not effective in prolonging incubation times of intracerebrally infected TSE animals (1, 7). Our findings regarding quinine, which is a quinacrine-related chemical, appear to be inconsistent with their findings about quinacrine. However, differences in the structures of the chemicals and in the administration routes, doses, and durations as well as experimental models might have caused this gap but it remains to be elucidated.

Biquinoline was 1,000 times more effective than quinine in inhibiting PrPres formation *in vitro* with respect to the IC_{50} value, but when initiated from an early stage with intraventricular injections of 1.6 nmol/day or intraperitoneal injections of 0.39 mmol/day, its effectiveness in prolonging incubation times *in vivo* was clear, albeit marginal. The stability of chemicals and accessibility to targets *in vivo* might be different between these chemicals, and the reason for the gap between inhibiting activity *in vitro* and therapeutic activity *in vivo* remains to be found.

In investigations of the immunohistochemistry of the post-mortem materials, abnormal PrP deposition in the white matter adjacent to the ventricle (where a chemical was injected continuously) was less evident in the mice treated with quinine or biquinoline from an early stage than in the control, although abnormal PrP deposition in the thalamus and hypothalamus was demonstrated in a fashion similar to that seen in the control. This would seem to imply that following treatment with a chemical, prolongation of incubation times in mice treated with the chemical might be associated with a reduction in abnormal PrP deposition in the brain.

In conclusion, we have demonstrated that quinoline derivatives with a relatively large side chain with a nitrogen are able to inhibit PrPres accumulation in ScNB cells and can prolong

the incubation periods of infected mice. The inhibition was not caused by interference in the biosynthesis or turnover of PrPsen or by the chelation of metals. Some of the chemicals, including quinine, are already in clinical use and are known to pass the blood-brain barrier. Thus, these drugs might be immediately available for clinical trials in investigations of the treatment of human TSEs.

ACKNOWLEDGMENTS

This study was supported by grants to K.D. from the Ministry of Health, Labor and Welfare (H13-kokoro-025) and from the Ministry of Education, Culture, Sports, Science and Technology (13557118, 14021085), Japan.

We thank B. Chesebro and R. Race in the Rocky Mountain Laboratories, NIAID for providing Tg7 mice, C. Weissmann in the Imperial College School of Medicine at St. Mary's, United Kingdom for Tg20 mice, and S. Katamine and S. Sakaguchi in Nagasaki University, Nagasaki, Japan, for PrP121-231. We also thank N. Suzuki in Daiichi Pharmaceuticals, Tokyo, Japan, for screening the chemical database.

REFERENCES

1. Barret, A., F. Tagliavini, G. Forloni, C. Bate, M. Salmona, L. Colombo, A. De Luigi, L. Limido, S. Suardi, G. Rossi, F. Auvre, K. T. Adjou, N. Sales, A. Williams, C. Lasmezas, and J. P. Deslys. 2003. Evaluation of quinacrine treatment for prion diseases. *J. Virol.* 77:8462-8469.
2. Brown, D. R., F. Hafiz, L. L. Glasssmith, B. S. Wong, I. M. Jones, C. Clive, and S. J. Haswell. 2000. Consequences of manganese replacement of copper for prion protein function and proteinase resistance. *EMBO J.* 19:1180-1186.
3. Brown, D. R., K. Qin, J. W. Herms, A. Madlung, J. Manson, R. Strome, P. E. Fraser, T. Kruck, A. von Bohlen, W. Schulz-Schaeffer, A. Giese, D. Westaway, and H. Kretzschmar. 1997. The cellular prion protein binds copper *in vivo*. *Nature* 390:684-687.
4. Brown, P., M. Preece, J. P. Brandel, T. Sato, L. McShane, I. Zerr, A. Fletcher, R. G. Will, M. Pocchiari, N. R. Cashman, J. H. d'Aignaux, L. Cervenkova, J. Fradkin, L. B. Schonberger, and S. J. Collins. 2000. Iatrogenic Creutzfeldt-Jakob disease at the millennium. *Neurology* 55:1075-1081.
5. Caughey, B., and G. J. Raymond. 1993. Sulfated polyanion inhibition of scrapie-associated PrP accumulation in cultured cells. *J. Virol.* 67:643-650.
6. Cherny, R. A., C. S. Atwood, M. E. Xilinas, D. N. Gray, W. D. Jones, C. A. McLean, K. J. Barnham, I. Volitakis, F. W. Fraser, Y. Kim, X. Huang, L. E. Goldstein, R. D. Moir, J. T. Lim, K. Beyreuther, H. Zheng, R. E. Tanzi, C. L. Masters, and A. L. Bush. 2001. Treatment with a copper-zinc chelator markedly and rapidly inhibits beta-amyloid accumulation in Alzheimer's disease transgenic mice. *Neuron* 30:665-676.
7. Collins, S. J., V. Lewis, M. Brazier, A. F. Hill, A. Fletcher, and C. L. Masters.

2002. Quinacrine does not prolong survival in a murine Creutzfeldt-Jakob disease model. *Ann. Neurol.* 52:503-506.
8. Doh-ura, K., T. Iwaki, and B. Caughey. 2000. Lysosomotropic agents and cysteine protease inhibitors inhibit scrapie-associated prion protein accumulation. *J. Virol.* 74:4894-4897.
 9. Doh-ura, K., E. Mekada, K. Ogomori, and T. Iwaki. 2000. Enhanced CD9 expression in the mouse and human brains infected with transmissible spongiform encephalopathies. *J. Neuropathol. Exp. Neurol.* 59:774-785.
 10. Fischer, M., T. Rulicke, A. Raeber, A. Sailer, M. Moser, B. Oesch, S. Brandner, A. Aguzzi, and C. Weissmann. 1996. Prion protein (PrP) with aminoproximal deletions restoring susceptibility of PrP knockout mice to scrapie. *EMBO J.* 15:1255-1264.
 11. Korth, C., B. C. May, F. E. Cohen, and S. B. Prusiner. 2001. Acridine and phenothiazine derivatives as pharmacotherapeutics for prion disease. *Proc. Natl. Acad. Sci. USA* 98:9836-9841.
 12. McKenzie, D., J. Bartz, J. Mirwald, D. Olander, R. Marsh, and J. Aiken. 1998. Reversibility of scrapie inactivation is enhanced by copper. *J. Biol. Chem.* 273:25545-25547.
 13. Miura, T., A. Hori-i, H. Mototani, and H. Takeuchi. 1999. Raman spectroscopic study on the copper(II) binding mode of prion octapeptide and its pH dependence. *Biochemistry* 38:11560-11569.
 14. Priola, S. A., A. Raines, and W. S. Caughey. 2000. Porphyrin and phthalocyanine antiscrapie compounds. *Science* 287:1503-1506.
 15. Prusiner, S. B. 1991. Molecular biology of prion diseases. *Science* 252:1515-1522.
 16. Race, R. E., B. Caughey, K. Graham, D. Ernst, and B. Chesebro. 1988. Analyses of frequency of infection, specific infectivity, and prion protein biosynthesis in scrapie-infected neuroblastoma cell clones. *J. Virol.* 62:2845-2849.
 17. Race, R. E., S. A. Priola, R. A. Bessen, D. Ernst, J. Dockter, G. F. Rall, L. Mucke, B. Chesebro, and M. B. Oldstone. 1995. Neuron-specific expression of a hamster prion protein minigene in transgenic mice induces susceptibility to hamster scrapie agent. *Neuron* 15:1183-1191.
 18. Viles, J. H., F. E. Cohen, S. B. Prusiner, D. B. Goodin, P. E. Wright, and H. J. Dyson. 1999. Copper binding to the prion protein: structural implications of four identical cooperative binding sites. *Proc. Natl. Acad. Sci. USA* 96:2042-2047.
 19. Will, R. G., J. W. Ironside, M. Zeidler, S. N. Cousens, K. Estibeiro, A. Alperovitch, S. Poser, M. Pocchiarri, A. Hofman, and P. G. Smith. 1996. A new variant of Creutzfeldt-Jakob disease in the UK. *Lancet* 347:921-925.